ALMA MATER STUDIORUM - UNIVERSITÀ DI BOLOGNA

SCUOLA DI INGEGNERIA E ARCHITETTURA

DIPARTIMENTO DI INGEGNERIA INDUSTRIALE

CORSO DI LAUREA MAGISTRALE IN INGEGNERIA MECCANICA

TESI DI LAUREA

in
LABORATORIO DI MECCANICA DEI TESSUTI BIOLOGICI

IN SILICO METHODS TO EVALUATE FRACTURE RISK AND BONE MINERAL DENSITY CHANGES IN PATIENTS UNDERGOING TOTAL HIP REPLACEMENT

CANDIDATO

Andrea Menichetti

RELATORE

Chiar.mo Prof. *Luca Cristofolini*

CORRELATORI

Prof. *Paolo Gargiulo*
Prof. *Magnús Kjartan Gíslason*

Anno Accademico 2015/16

I° Sessione

Alla mia famiglia

Abstract

Total Hip Replacement is one of the most successful operations. There are two variants of the prosthesis that differ in the way the implant is anchored to the bone: cemented (fixed by bone cement) and cementless (fixed by press-fitting).
Currently, surgeons do not have any quantitative guideline for choosing between the two typologies, basing the decision just on their experience.
Two of the issues affecting cementless prostheses are the possibility of intra-operative fracture during the press-fitting and the bone resorption after the operation.
Starting from densitometric measurements on CT images of patients that underwent cementless total hip replacement, two methods were developed: 1) to assess the risk of intra-operative fracture by means of a finite element analysis; 2) to evaluate bone mineral density changes (three-dimensionally around the prosthesis) 1 year after the operation.
A cohort of 5 patients was selected to test both procedures. Each patient was CT-scanned in three different time steps: one before the operation and the other two 24 hours and 1 year post-operatively.
The obtained results confirmed the feasibility of both methods, and allowed to distinguish and quantify the differences between the patients.
The feasibility of both methodologies suggests the possibility to use them in a clinical ambit: 1) knowing the risk of intra-operative fracture may provide clinicians with a guideline for the optimal implant decision-making; 2) knowing bone mineral density changes 1 year post-operatively may be used as a monitoring tool during the follow-up.

Keywords: Total Hip Replacement, Cementless Prosthesis, Intra-operative Fracture Risk; Bone Mineral Density; Finite Element Analysis.

Abstract

La sostituzione totale d'anca è uno degli interventi chirurgici con le più alte percentuali di successo. Esistono due varianti di protesi d'anca che differiscono in base al metodo di ancoraggio all'osso: cementate (fissaggio tramite cemento osseo) e non cementate (fissaggio tramite forzamento). Ad oggi, i chirurghi non hanno indicazioni quantitative di supporto per la scelta fra le due tipologie di impianto, decidendo solo in base alla loro esperienza.
Due delle problematiche che interessano le protesi non cementate sono la possibilità di frattura intra-operatoria durante l'inserimento forzato e il riassorbimento osseo nel periodo di tempo successivo all'intervento.
A partire da rilevazioni densitometriche effettuate su immagini da TC di pazienti sottoposti a protesi d'anca non cementata, sono stati sviluppati due metodi: 1) per la valutazione del rischio di frattura intra-operatorio tramite analisi agli elementi finiti; 2) per la valutazione della variazione di densità minerale ossea (tridimensionalmente attorno alla protesi) dopo un anno dall'operazione.
Un campione di 5 pazienti è stato selezionato per testare le procedure. Ciascuno dei pazienti è stato scansionato tramite TC in tre momenti differenti: una acquisita prima dell'operazione (pre-op), le altre due acquisite 24 ore (post 24h) e 1 anno dopo l'operazione (post 1y).
I risultati ottenuti hanno confermato la fattibilità di entrambi i metodi, riuscendo inoltre a distinguere e a quantificare delle differenze fra i vari pazienti.
La fattibilità di entrambe le metodologie suggerisce la loro possibilità di impiego in ambito clinico: 1) conoscere la stima del rischio di frattura intra-operatorio può servire come strumento di guida per il chirurgo nella scelta dell'impianto protesico ottimale; 2) conoscere la variazione di densità minerale ossea dopo un anno dall'operazione può essere utilizzato come strumento di monitoraggio post-operatorio del paziente.

Parole chiave: Sostituzione Totale d'Anca, Protesi Non Cementata, Rischio di Frattura Intra-operatorio, Densità Minerale Ossea, Analisi agli Elementi Finiti

Abbreviations

BMD = Bone Mineral Density

CT = Computed Tomography

DEXA = Dual Energy X-ray Absorptiometry

DICOM = Digital Imaging and COmmunications in Medicine

EMG = Electromyography

FE = Finite Element

FEA = Finite Element Analysis

FEM = Finite Element Method

FR = Fracture Risk

FRI = Fracture Risk Index

GV = Gray Values

GVr = Resulting GV

GV1 = GV of Dataset 1

GV2 = GV of Dataset 2

HA = Hydroxyapatite

HU = Hounsfield Unit

OECD = Organization for Economic Co-operation and Development

PMMA = Polymethylmethacrylate

Post 24h = CT-Scan 24 hours after the THA operation

Post 1y = CT-Scan 1 year after the THA operation

Pre-op = CT-Scan before the THA operation

PVE = Partial Volume Effect

ROI = Region of Interest

RU = Reykjavik University

STL = Stereo Litography Interface Format

THA = Total Hip Arthroplasty

THR = Total Hip Replacement

UHMWPE = Ultra High Molecular Weight Polyethylene

WHO = World Health Organization

XLPE = Cross-linked Polyethylene

List of figures

Figure 1.1: Project Timeline 2

Figure 1.2 : The structure of a long bone (femur) 4

Figure 1.3 : Cortical and Trabecular Bone in proximal femur. [13] 5

Figure 1.4: The Haversian System [14] 6

Figure 1.5 : Bone Remodeling Phases 7

Figure 1.6 : Direction of trabeculae in proximal femur. Red arrows represent daily loads 8

Figure 1.7 : a) Healthy Trabecular Bone vs. b) Osteoporotic Trabecular Bone 9

Figure 1.8 : Load direction of body weight 10

Figure 1.9 : Anatomy of the Hip Joint [25] 11

Figure 1.10 : Movements of Hip Joint [26] 12

Figure 1.11 : Statistic on THR, according to [32] 13

Figure 1.12 : Components of THA. From [34] 14

Figure 1.13: Surgical technique to insert cementless stem. Adapted from [46] 18

Figure 1.14 : Cemented (a) vs. Non-cemented (b) stems. Retrieved from [48] 19

Figure 1.15: Illustration of Helical Tomography delivery 21

Figure 1.16 : Scheme of the attenuation principle 22

Figure 2.1: Study Workflow 26

Figure 2.2: Philips' Brilliance 64-slice CT scanner 29

Figure 2.3: A) CT-slice of a post-op THR, with artifacts due to the metallic stem. B) The same CT-slice after artifact reduction: no streaks are now present. [10].....29

Figure 2.4 : BMD vs. HU relationship.....30

Figure 2.5 : Steps to create the 3D model.....32

Figure 2.6 : Convergence Test.....34

Figure 2.7 : Volume mesh of the femur model.....34

Figure 2.8 : Materials Histogram.....36

Figure 2.9 : Material Distribution.....36

Figure 2.10 : Boundary Conditions.....37

Figure 2.11 : External loads directions in previous model [53].....37

Figure 2.12 : Dynamic model of implant insertion [74].....39

Figure 2.13 : Force over time profile of the implant being hit by one hammer blow [74].....40

Figure 2.14 : Trend of the force over time on the implant after n hammer blows [74].....40

Figure 2.15 : a) Model of the bone-stem conic coupling with forces involved in the system. b) Forces polygon for the equilibrium.....41

Figure 2.16 : Clipped view of the meshed femur.....43

Figure 2.17 : Lf referring to Zimmer® rasp 44

Figure 2.18 : Measurements to calculate per_m 45

Figure 2.19 : The 7 zones for FR, according to [10] Greater Trochanter zone is evaluated in the lateral side of the bone. 46

Figure 2.20 : Different femur positions between Post 24h (a) and Post 1y (b). 47

Figure 2.21 : Mimics project before Reslicing 48

Figure 2.22 : Mimics project after Reslicing 49

Figure 2.23: Femur bone mask (highlighted in purple) 50

Figure 2.24: 5 Regions of Interest for BMD, from [79] 50

Figure 2.25 : Point-based Image Registration.....51

Figure 2.26 : Landmarks for Registration. Landmark 1 (stem's tip) not visible.....52

Figure 2.27 : Subtract Fusion Method (in this specific case, Post 24h - Post 1y) 53

Figure 2.28 : Steps to evaluate bone loss/gain.....55

Figure 3.1: Results of FE analysis: Max Principal Elastic Strain Distribution.....57

Figure 3.2 : Fracture Risk Indexes for different anatomical regions of the proximal femur plotted against patients' age 58

Figure 3.3 : HU distribution over the mask of the operated femur's 3D model. Cancellous and cortical peaks are indicated.....59

Figure 3.4 : Number of fractured elements against average density of cortical bone 60

Figure 3.5 : Number of fractured elements against average density of trabecular bone 60

Figure 3.6 : % BMD changes in ROI.....65

Figure 4.1 : Radiography taken a few days after cementless THR, demonstrating a possible intra-operative fracture. Courtesy of Landspitali – University Hospital of Iceland 82

Figure A-1 : The Zimmer's CLS® Spotorno® Stem [86] 98

List of tables

Table 1.1: Summary of the most-used materials in THR. Adapted from [35] 16

Table 2.1 : Subjects' Info 28

Table 2.2 : Convergence Test results 33

Table 2.3 : Applied Pressure for FRI assessment 45

Table 2.4 : Subtraction Fusion Method.....52

Table 3.1: FRI in the 7 areas of investigation 58

Table 3.2 : Average BMD [mg/cm3] 61

Table 3.3 : Cortical BMD [mg/cm3].....61

Table 3.4: BMD loss/gain volume fractions 66

Table 3.5 : BMD loss/gain volume fractions in ETH protocol 67

Table A-1 : Properties of Protasul-100 (Ti-6Al-7Nb) [87].....98

Contents

Abstract (ENG) iii

Abstract (ITA) iv

Abbreviations v

List of figures vii

List of tables x

1. **Introduction** 1

1.1 Project Presentation 1

1.2 Theoretical Background 3

1.2.1 The Bone 3

1.2.2 The Hip Joint 10

1.2.3 Total Hip Replacement 12

1.2.4 Basic Principles of Computed Tomography 21

1.3 Aim of the Thesis 23

1.3.1 Fracture Risk Assessment 24

1.3.2 Bone Mineral Density Changes 25

2. **Materials and Methods** 26

2.1. Study Workflow 26

2.2. Data Acquisition 27

2.2.1. Subjects Information 27

2.2.2. CT Acquisition 28

2.2.3. CT Calibration 30

2.3. Fracture Risk Index 31

2.3.1. Segmentation 31

2.3.2. 3D Modeling 31

2.3.3. FE Modeling 32

2.3.3.1. Material Assignment 35

2.3.3.2. Boundary Conditions 36

2.3.4. Fracture Risk Index Evaluation 46

2.4. Bone Mineral Density Changes 47

2.4.1. Reslicing 47

2.4.2. Segmentation 49

2.4.3. Image Registration and Subtraction 51

2.4.4. Bone Mineral Density Gain and Loss Evaluation 53

3. **Results** 56

3.1. Fracture Risk Index 56

3.2. Bone Mineral Density Changes 61

3.2.1 BMD changes: 5 ROI 62

3.2.2 BMD changes: volume fractions 66

3.2.3. Comparison between two protocols 67

4. **Discussion** 81

4.1. Fracture Risk 81

4.2. Bone Mineral Density Changes 83

5. **Future work and Conclusions** 86

5.1. Fracture Risk 86

5.2. Bone Mineral Density Changes 87

References 88

Appendix A-1 97

The CLS® Spotorno® Stem 97

Acknowledgments 99

1. Introduction

1.1 Project Presentation

Total Hip Replacement (THR) is a widely used and successful orthopedic procedure for the treatment of many crippling diseases that cause advanced damage of hip joints, such as osteoarthritis, femoral neck's osteonecrosis and femoral neck's fractures.
THR consists of replacing the articular components (both femoral and acetabular) with artificial ones, in order to relieve patients of pain and re-establish mobility, leading also to a considerable improvement in terms of life quality.
There are two types of THR methodological options, that differ in the way the prosthesis is fixed to the bone, that is to say with or without the use of the bone cement.
In cemented THR, acrylic bone cement ensures the fixation of the implant, while in cementless THR the primary stability is secured by geometrical interlocking, press-fit forces and friction between bone and implant.
The bone behaves differently depending on which implant typology is used, but there is not an absolute criterion for choosing between cemented and cementless THR, indeed large studies have shown different results in terms of clinical outcome and the issue is still debated [1], [2], [3], [4].
For instance, in the first years following the operation, cases of revision surgery due to periprosthetic fractures are more frequent for cementless implants [2]. However, a revision surgery is much more critical for cemented implants, since residual cemented bone can be removed during cement extraction from the femoral canal.
Moreover, knowing that bone adapts in correlation to the loads upon it (Wolff's law), the use of the cement reduces the mechanical stress around the prosthesis, leading to a gradual decrease of the bone mineral density and a consequent raise of the risk of aseptic loosening of the stem [5], [6].
On the other side, the uncemented stem allows a preload of the layer immediately adjacent to the stem and therefore bone is encouraged to grow [7].
Another important consideration is that not every patient is able to withstand the press-fitting operation to insert the cementless stem, since if bone is not strong enough, intra-operative fracture may occur.
It is clear that clinicians deal with an important issue when choosing between the two

methodologies, however, presently, there is a lack of a robust, quantitative method to guide physicians to the choice of the proper implant for the patient. In fact, for implant decision making, surgeons usually rely on their experience, just basing on possible bone quality indicators such as age, gender and qualitative assessment of CT images.
This means that generally younger and healthier patients receive cementless implants, while over-65 ones usually get cemented prosthesis.
Nevertheless, it has been clearly shown that other factors, such as bone mineral density and muscle strength play a crucial role in the predisposition to one implant or another. These factors depends not only on age and gender, but also on patient's lifestyle and genetics [8].

In this context, Landspítali – University Hospital of Iceland and the Reykjavík University started a synergic collaboration to develop a project which aims to establish a subject-specific clinical evaluation score for total hip replacement planning and for post-operative assessment, with the final aims of both improving patient mobility and reducing healthcare costs of revision surgeries.
This project [9] proposes a novel approach for clinical assessment by collecting unique data. Specific objectives of the project are:
1) to develop monitoring techniques based on gait analysis and electromyography (EMG);
2) to develop assessment methods for bone and muscle density starting from CT scans;
3) to develop and further validate computational processes based on 3D modeling and finite element method (FEM) to estimate mechanical stress acting on femurs and therefore to help selecting the optimal surgical technique;
4) to develop evaluation methods to check bone remodeling short and long-term after THR.
Acquisition, elaboration and analysis of the patient's data follow a standard protocol, whose workflow is resumed in Fig. 1.1. The output from all the elaborations will be correlated to the chosen implant type, to patients anamnesis and rehabilitation results.

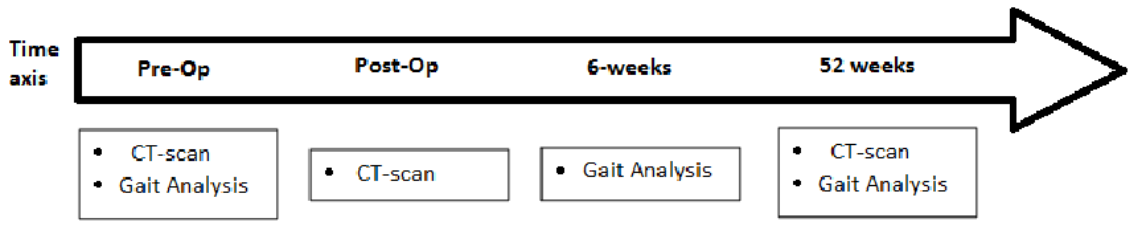

Figure 1.1: Project Timeline

A few days before surgery, patients are CT-scanned and undergo a gait assessment. Right after the operation, they undergo another CT-scan. Then, 6 weeks later, patients are called in for gait measurements. 52 weeks post-operatively, they are checked with another CT-scan and gait analysis. Finally collected data are analyzed. [10]

The work presented in this paper is included in the frame of the above-mentioned project and specifically concerns two themes: 1) to improve the assessment method, by means of a finite element analysis (FEA), for the femur's risk of fracture during the press-fitting of the non-cemented stem and 2) to develop a novel procedure to evaluate bone mineral density changes around the prosthesis one year after surgery.
Both assessment methods are based on data from CT-scans acquired in 3 different time steps: one before the operation and the other two 24 hours and 1 year post-operatively.
CT-scans allow to quantify the quality of the patient's femur in terms of bone mineral density, that is the basic information which both methods are developed with.

1.2 Theoretical Background

1.2.1 The Bone

The bone is a connective tissue whose peculiar feature is to have a mineralized extra-cellular matrix, which gives it stiffness and mechanical strength.
Bone is composed of 65% by inorganic component and 35% by organic matrix, cells and water.
Organic component is principally made of collagen, the rest is non-collagenic proteins. The mineral component mainly consists of *hydroxyapatite* (HA), namely calcium apatite, $Ca_{10}(PO_4)_6(OH)_2$, that is present in little crystals (length: 20-40 nm; thickness: 1-1.5 nm) between collagen fibrils. The organic is the tough and flexible component, while the mineral is the brittle and stiff one.
Bone's functions are both mechanical and physiological. Mechanical tasks of the bones are to support the body (they form the skeletal system), to protect vital organs, to transfer loads and, in synergy with muscles, to produce motion of the limbs and the entire body. Physiologically speaking, bones are the primary site of hemopoiesis, as formation of blood cells takes place in the bone marrow. Bones are also the major calcium storage of the body, and they play an important role in the regulation (homeostasis) of this fundamental element for several vital processes.

Anatomy of the bone

Human adult skeleton counts 206 bones with different shape and dimensions.
For the purpose of this study, just long bones will be considered, since femur belongs to this category.
The anatomy of a long bone is depicted in Fig. 1.2.

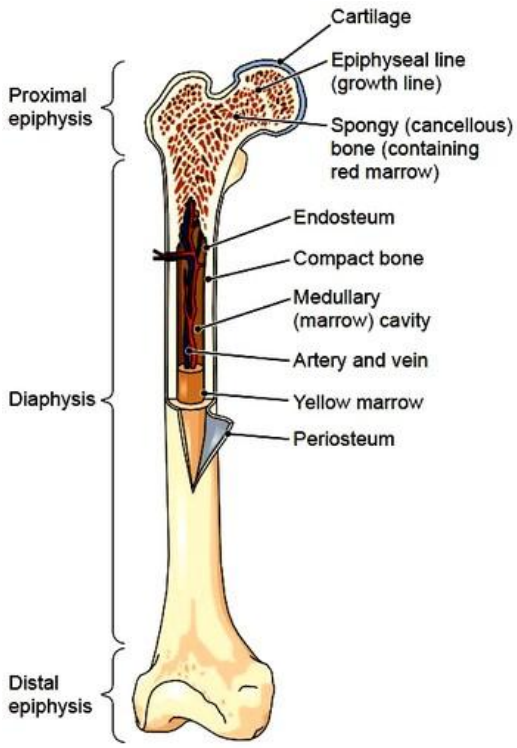

Figure 1.2 : The structure of a long bone (femur)

In adults, the long bone is made up of a central hollow part with an approximately cylindrical shape, called *diaphysis*. The extremities, called *epiphysis*, are wider, rounded and are covered by a cartilaginous tissue (hyaline cartilage) that reduces friction with adjacent bone segment forming the joint. Intermediate regions between diaphysis and epiphysis are named *methapysis.*
The external surface of bone segment, wherever it is not covered by articular cartilage, is called *periosteum*. It is widely vascularized and has a layer rich of active cells and elastic fibers. It also plays an important role in the remodeling process of the bone. The canal in the middle of long bones is called the *medullary canal*. The thin layer that surrounds the surface of these canals is called *endosteum*, which mainly consists of bone-forming cells. [11]

Structures of bone tissue

At a microscopical level, adult bone is organized in a modular structure made of adjacent layers, known as *lamellae*, in which collagen fibrils are oriented in parallel plans. Each lamella has a thickness of about 3-7 μm. Orientation of fibrils in adjacent layers is different, building a plywood-like structure.

Macroscopically, adult human bone is organized into two different architectonical structures: *cortical* (*compact*) bone and *cancellous* (*spongy* or *trabecular*) bone. (Fig. 1.3)

Cortical bone, which contributes about 80% of the skeletal mass, has a solid and compact structure, and it constitutes the external part of diaphysial and epiphyseal areas.

Cancellous bone has a porous structure since it is made of a network of little irregularly-shaped rods and plates, named *trabeculae*; it is mainly present in the epiphyseal regions and hosts red bone marrow – where blood cells are produced – in its interstices.

Cortical bone is heavier, stiffer and stronger, while trabecular one is lighter, less dense and with low mechanical strength properties.

Mechanically, a thin shell of cortical bone internally filled with spongy bone constitute an optimal integrated architecture, since cortical bone has the task to withstand loads, while cortical bone sustains the shell and prevents from buckling. [12]

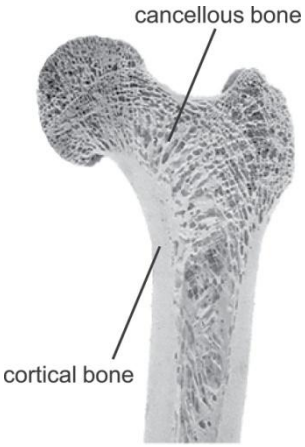

Figure 1.3 : Cortical and Trabecular Bone in proximal femur. [13]

In cortical bone, a packet of 4-30 concentric lamellae is arranged to surround a central cavity, called *haversian canal*, that is a longitudinal canal filled with blood and lymphatic vessels

and nerves. The haversian canals are interconnected by transverse canals, also called *Volkmann canals*, which allow the communication with the periosteum and bone marrow. The system made up by lamellae and haversian canal is called *osteon* or *haversian system*; it represents the structural unit of cortical bone and its characteristic diameter is 200-250 μm. Externally to the osteon, there is a 1-2 μm thick layer of mineralized matrix, deficient in collagen, called *cement line.*

Internally to the osteon's structure, there are little cavities, called *lacunae*, that host *osteocytes*, namely cells trapped during bone growth process. Lacunae are interconnected by a network of little canals, called *canaliculi.* (Fig. 1.4)

In addition to osteons, lamellae can also organize themselves in other two different structures: *circumferential lamellae* (continuously surrounding bone's body) and *interstitial lamellae* (fragment of residual osteons, filling the gaps between complete osteons). (Fig. 1.4)

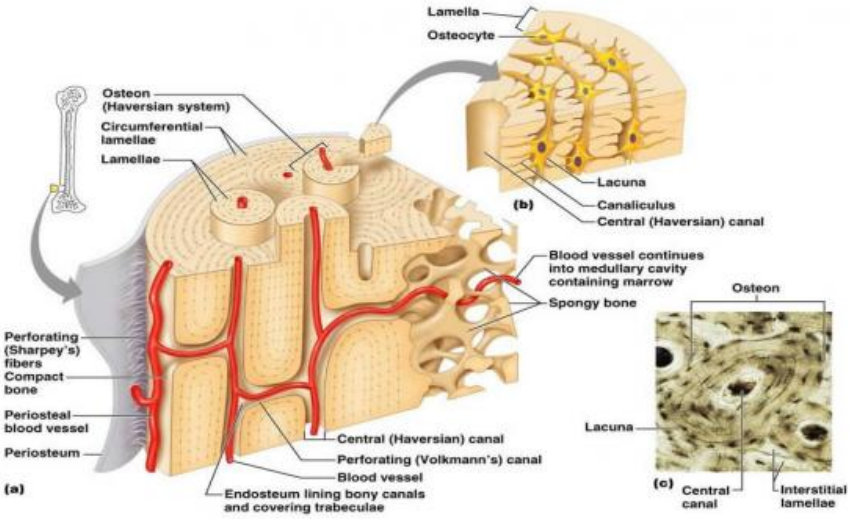

Figure 1.4: The Haversian System [14]

Trabecular bone's structural unit is the *trabecular packet*, a set of lamellae arranged in thin columns, 50-600 μm thick and circa 1 mm long. Similarly to compact bone, cement lines keep trabecular packets together. [15]

Bone modeling and remodeling

Bone is a dynamic tissue that undergoes continual adaption during life to preserve skeletal size, shape, and structural integrity and to regulate mineral homeostasis. Two processes, remodeling and modeling, allow development and maintenance of the skeletal system. Bone modeling is responsible for growth and mechanically induced adaption of bone and requires that the processes of bone formation and bone removal (resorption), although globally coordinated, occur independently at distinct anatomical locations. Bone remodeling is responsible for removal and repair of damaged bone to maintain integrity of the adult skeleton and mineral homeostasis. [16]

Main actors involved in these processes are *osteoclasts* (poly-nuclear cells assigned to bone lysis, by chemically attacking HA and removing collagen), *osteoblasts* (mono-nuclear cells assigned to bone formation, by synthesizing and secreting non-mineralized matrix, named *osteoid*) and *osteocytes* (the most numerous cells in mature bone, former osteoblasts trapped in the just-created osteoid).

During remodeling process, old bone is resorbed by osteoclasts and replaced with new osteoid. First osteoclasts are activated, and the resorption phase takes approximately 10 days. Following resorption, macrophage-like cells are found at the remodeling site in the reversal phase.

Osteoblast precursors are then recruited, which proliferate and differentiate into mature osteoblasts, before secreting new bone matrix. The matrix then mineralizes to generate new bone and this completes the remodeling process. (Fig. 1.5)

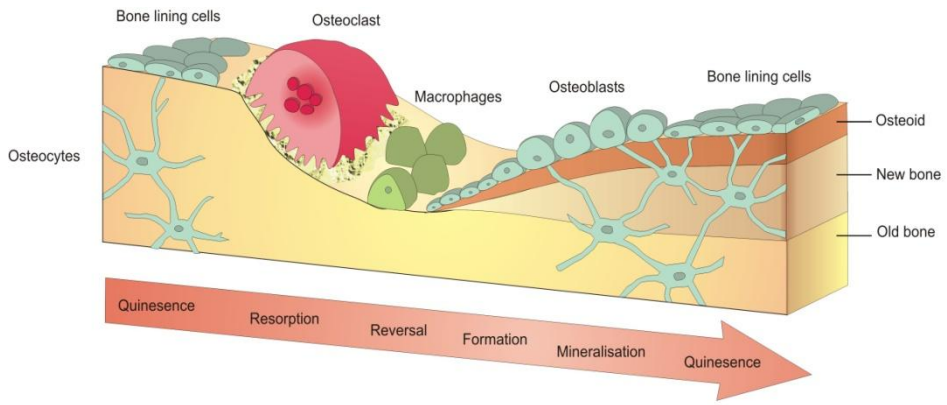

Figure 1.5 : Bone Remodeling Phases

Copyright of Biomedical Tissue Research, University of York

It has been found that bone remodeling is not equal for different anatomical sites, even for the same bone segment. Possible reason for this peculiarity is that remodeling process is guided by biomechanical factors. Basically, remodeling tends to maintain physiologically-loaded bone and to reduce bone that is under-loaded. This process involves both cortical and spongy bone: for instance, if bone undergoes loads that are under the physiological level, cortical bone's thickness diminishes (reducing the resistant section) and trabeculae's number and dimension decrease, in addition to a reduced mineralization of the matrix. In case of over physiological level loads, bone behaves in the opposite way. It has been proved that bone is able to adapt to mechanical cycling load conditions, both in direction and magnitude. [17], [18]

An emblematic example of this adaptability is provided by the proximal epiphysis of the femur (Fig. 1.6), in which trabeculae of the cancellous bone are aligned following daily loads direction.

It has been also shown that bones are optimized structures. In fact they are able to withstand daily loads and variations of the same with a rather uniform margin of safety and with a minimal mass. [19].

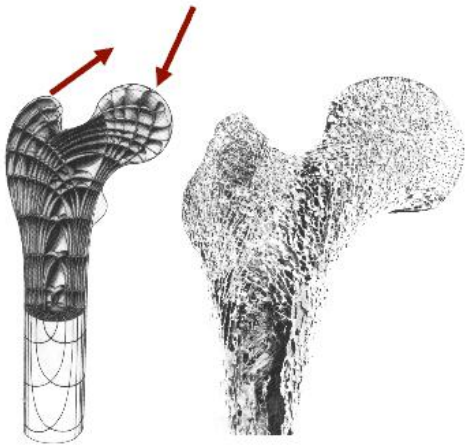

Figure 1.6 : Direction of trabeculae in proximal femur. Red arrows represent daily loads.

Also aging contributes to the variation of bone structure. Basically, aging has a double effect: loss of bone mass and brittleness. The first effect results from the demineralization of bone matrix; this happens earlier and has generally a faster degradation rate for women [20]. The second principal effect of aging on the skeletal system, brittleness, results from deteriorated mechanical integrity of the collagen network, that gives the bone its toughness. This leads the bone to be more susceptible to fracture. As result of aging, for instance, cancellous bone's

trabeculae become less dense and thinner (Fig. 1.7), while dimensions of cortical bone – both internal and external diameter – raise in order to compensate the loss of mechanical strength by increasing the resistant section. This condition can be classified as *osteoporosis.* [21], [22]

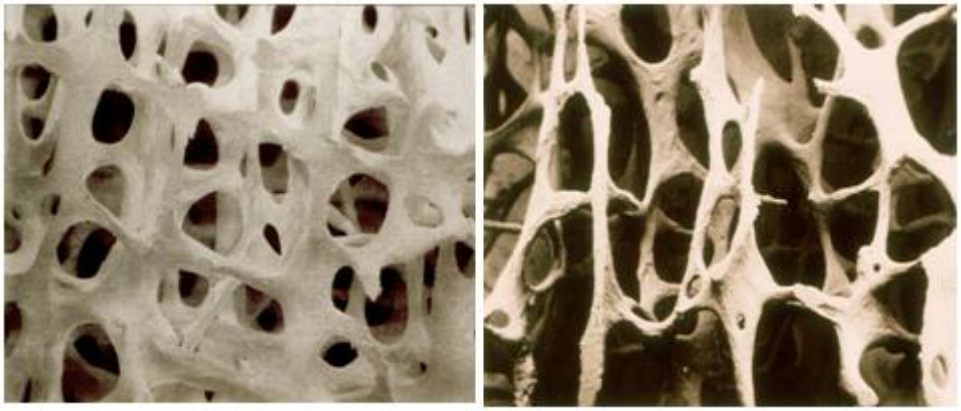

a) **b)**

Figure 1.7 : a) Healthy Trabecular Bone vs. b) Osteoporotic Trabecular Bone

Remodeling process is fundamental also for bone – prosthesis interaction.
With regard to THR, since metal implant is much stiffer than the femur, the load transferring through the bone changes, if compared to the preoperative mechanical conditions.
As a consequence, the stem shields the bone – in certain regions – from the stresses it used to be subject. This phenomenon is known as *stress shielding*. The reduction of the mechanical stimulus to the bone surrounding the stem causes bone resorption, which can consequently compromise stem's stability and eventually result in implant's failure. [5] [23] [24]
Fig. 1.8 gives a schematic indication on how body weight stress is unloaded in the femoral bone after THR.

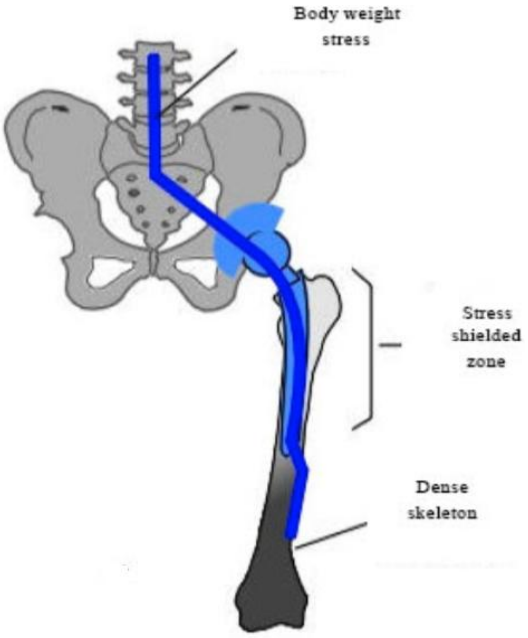

Figure 1.8 : Load direction of body weight

The stem is stiffer than the bone, this causes stress shielding in the proximal femur, with consequent bone mineral density decrease. Femur remains dense distally to the stem.

1.2.2 The Hip Joint

The hip joint (coxal) is a ball-and-socket synovial type joint that connects the lower limb to the pelvic girdle.

The hip joint consists of an articulation between the head of femur and acetabulum of the pelvis.

The acetabulum is a cup-like depression in the lateral side of the pelvis. The head of femur is hemispherical, and fits completely into the concavity of the acetabulum. Both the acetabulum and head of femur are covered with articular cartilage, acting like a cushion to compressive forces and lubricating the joint.

The hip joint is designed to have a great stability, since it has to withstand body's weight and transfer it to the lower extremities. This is achieved with the strong muscles and ligaments covering the joint, along with the good fit of the femoral head inside the acetabulum. (Fig. 1.9)

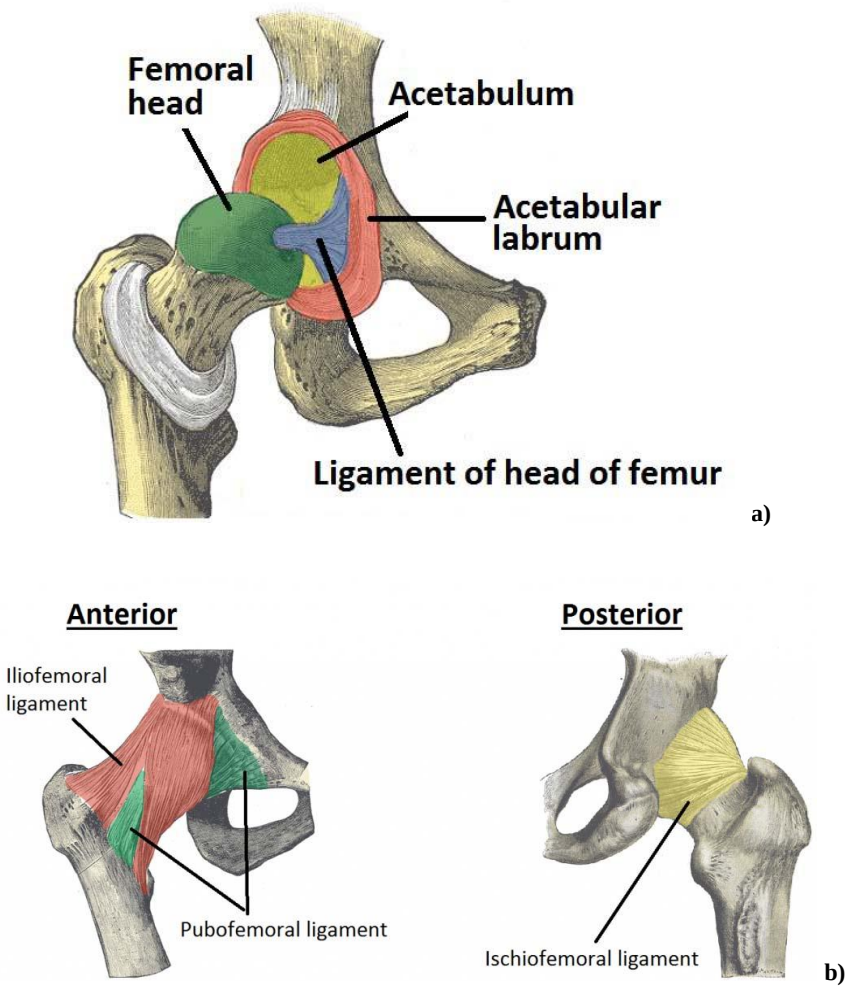

Figure 1.9 : Anatomy of the Hip Joint [25]

a) Femural Head and Acetabulum of the hip joint; b) Extracapsular ligaments: they prevent excessive hyperextension (Iliofemoral), excessive abduction and extension (Pubofemoral), excessive extension of the femur (Ischiofemoral).

The movements that can be carried out at the hip joint are flexion/extension, abduction/adduction and medial/lateral rotation. (Fig. 1.10) The degree to which flexion at the hip can occur depends on whether the knee is flexed, which relaxes the hamstrings, and increases the range of flexion. Extension at the hip joint is limited by the joint capsule, and in particular, the iliofemoral ligament. These structures become taut during extension to limit further movement.

Figure 1.10 : Movements of Hip Joint [26]

1.2.3 Total Hip Replacement

THR is the indicated surgical solution to advanced hip joint diseases. Symptoms of hip joint condition counts stiffness, deformity, limb shortening and movement reduction.
Patients seek help from surgery in order to get rid of pain, restore range of motion and improve quality of life.
The most common diseases [27] that can lead to make the choice to undergo total hip arthroplasty (THA) are:

- *Osteolysis*: wear that leads to local loss of bone caused by different articular disorders;
- *Osteoarthritis*: degenerative arthritis disease characterized by breakdown of the joint's cartilage, leading to friction between ball and socket of the joint that causes severe pain. It is the most common diagnosis between patients undergoing THA; [28] [29]
- *Avascular Necrosis*: lack of blood supply into bone that can progressively lead to joint surface collapse that results in increasing pain;
- *Rheumatoid Arthritis*: chronic inflammatory disorder that involves inflammation in the lining of the joint and may result into cartilage destruction;
- *Femur's neck Fracture*;
- *Developmental Dysplasia*: femoral head has an abnormal relationship to the acetabulum;
- *Paget's Disease*: metabolic bone disorder that induces an increased and irregular formation of bone;
- *Tumor*.

Total hip replacement is one of the most successful and cost-effective interventions in medicine. [28]. Its success is well reported in literature and a survival rate - intended as maintaining the prosthesis in its initial condition - of about 90% is recorded at 15 years follow-up [29] [30] [31].

The most common causes of complications for THA are prosthesis dislocation, aseptic loosening of the stem and/or of the cup due to mechanical wear debris, periprosthetic bone fracture, septic loosening and breakage of the prosthesis (rare) [27] [29]. Most of these complications can directly lead to premature revision surgery, that is to say removal of the failed component and replacement with a new one.

Statistics of Emilia Romagna (Italy) [29] and the rest of the OECD countries [32] show that the number of hip replacements has increased rapidly since 2000. On average, the rate of hip replacements increased by about 35% between 2000 and 2013. (Fig. 1.11 b)

For instance, in Italy [33], number of yearly THR surgeries in 2001 was 45 656, while in 2012 became 62 153.

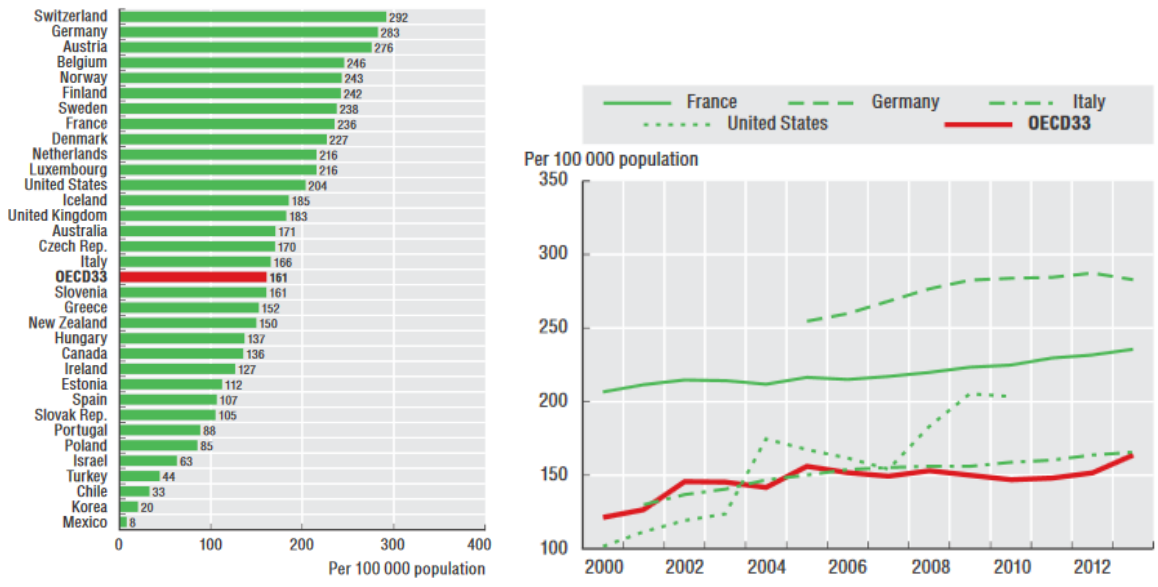

Figure 1.11 : Statistic on THR, according to [32]

a) Number of THR surgeries in 2013. Iceland counts 185 operations per 100 000 people, Italy 166; b) Trend in hip replacement surgery, for some selected countries, from 2000 to 2013. Average statistics for OECD countries are represented in red.

According to data collected between 2000 and 2014 in Emilia Romagna [29], average age at primary THA was 66.7 years; while the largest age group for primary THA was 70-79 years. Male's average age of patients that underwent hip replacement surgery in 2014 was 66.5 while female's was 70.2 . However, out of 87 993 patients that underwent primary THA during 2000-2014, 60% were female.

Prosthesis components

THA is the replacement of both articulating surfaces of a degenerated hip joint. In the conventional approach, the spherical part of the joint is completely replaced. The counterpart of the joint is also replaced by a semi-spherical shell. Artificial hip joints are innovative, high-quality biomedical engineering products. Prostheses are designed to last for at least 20 years, however their lifespan can be limited by wear.

There is a large variety of hip prostheses on the market in terms of material, shape, coating etc. due to the continuous research aiming to reduce the likelihood of post-operation complications; however, currently, there is a basic modular-design principle common for all of the

implants. (Fig. 1.12)

The damaged hip joint is replaced by two artificial components: the *acetabular cup* (socket) and the *femoral head* (ball). The latter is anchored in the femur by the *stem*, while the former is fixed in the pelvis. The acetabular cup consists of a *shell* in which a *liner* is inserted in order to provide the load bearing articulating surface.

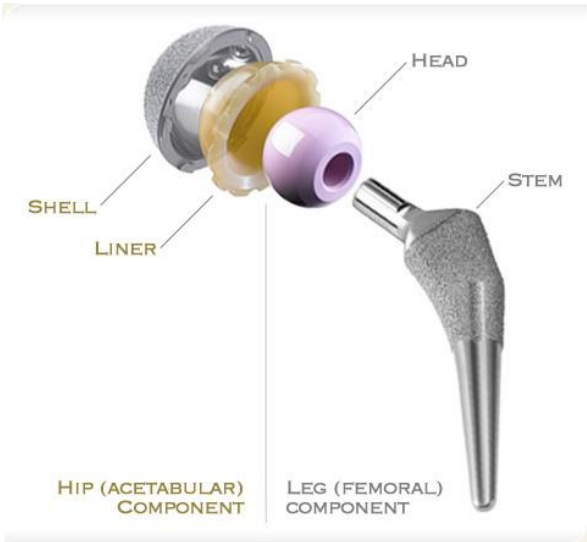

Figure 1.12 : Components of THA. From [34]

The modularity of the implant is justified by the fact that different materials with different properties need to be used to meet the different requirements for each component. Modularity can also allow the revision surgery of just the failed component, without replacing all the implant.
In order to take over the physiological function of a hip joint, a prosthesis must have three different compatibility requirements: [35]

- Structural: prosthesis must withstand millions of loading cycles, i.e. it must have an adequate mechanical strength and fatigue strength;
- Tribological: the articulating surfaces must not be compromised by wear, ensuring a correct relative motion of the 2 joint components;
- Biological: stem and shell must integrate well with the bone and resist to body's corrosive environment. Inevitable debris particles released due to wear must not harm the organism.

Hip prostheses can be categorized basing on the utilized materials for the combination femoral head-acetabular cup. The most common combinations are metal-on-polyethylene (MoP), metal-on-metal (MoM) and ceramic-on-ceramic (CoC).

The femoral stem is the component subjected to the highest mechanical stresses and it must provide a uniform transfer of the cycle loads from the prosthesis to the lower limb. Thus, the used material must have high mechanical strength and fatigue resistance, for this reason only metals have been considered to this application so far. Factors like stem length, stem cross-section and neck angle influence stability and therefore must be taken into account when designing it. [36] [37] [38] [39]

The femoral head is coupled to stem's neck through the latter's taper junction. Paramount factor is head's diameter, which plays a fundamental role in the achievable range of motion of the artificial joint, along with its stability. Design criteria for the femoral heads are: i) the minimum surface roughness to get lowest friction and wear rate possible; ii) the maximum outer diameter, to improve stability and range of motion [40]; iii) the mechanical resistance of the material to withstand tensile stresses generated along the taper junction. Metal and ceramic have been used as materials for femoral heads. Ceramic heads, if compared to metal ones, result to have more smoothness (thus less friction coefficient). On the other side there are limitations in manufacturing large diameters, along with higher brittleness.

The liner of the acetabular cup is the socket of the hip joint, being the counterpart of the femoral head. It represents the soft component of the hard-soft coupling, therefore it is manufactured in order to have its surface more worn out than femoral head's one, aiming to maintain relative motion in an acceptable range. The liner can be made of metal (CoCrMo) or ceramic, but it has been usually produced in UHMWPE (ultra high molecular weight polyethylene), which has allows low friction. However, UHMWPE presents high wear rates, that can be reduced by means of a gamma- or beta-ray irradiation technique (Crosslinked UHMWPE, also known as XLPE). [27] [41]

The acetabular cup's shell is secured to the pelvis either with bone cement or press-fitting and the fixation technique influences its external surface design: for instance, uncemented components have porous surface finishing (e.g. with sintered titanium beads) or HA coatings to promote osteointegration. [27] [36]
For MoP and CoC implants, shells must also provide mechanical stability for brittle ceramic or soft UHMWPE liners and is therefore mostly fabricated in pure titanium.

Table 1.1 resumes the most used materials to fabricate THR's components.

Component	Material Class	Most Used Material
Femoral Stem	Metal	CoCrMo-wrought, Ti-alloys, stainless steel
Femoral Head	Metal	CoCrMo-cast, stainless steel
	Ceramic	Alumina (pure or zirconia-toughened), zirconia
Acetabular Cup's Liner	Polymer	UHMWPE, XLPE
	Metal	CoCrMo-cast
	Ceramic	Alumina (pure or zirconia-toughened), zirconia
Acetabular Cup's Shell	Metal	Commercially pure Ti, stainless steel

Table 1.1: Summary of the most-used materials in THR. Adapted from [35]

As already mentioned in § 1.1, the fixation of the implant to the bones characterizes two different categories: *cemented* and *non-cemented* prostheses.
For the purpose of this thesis, attention will be put just into femoral stems, knowing that the same fixation techniques can be adopted for acetabular cup's shells too.

Cemented stem

Historically the first fixation typology (Sir John Charnley, 1961), cemented stems (Fig. 1.14 a) are secured to the femur through an acrylic bone cement. Usually, the material for the cement is Polymethylmethacrylate (PMMA). Actually, bone cement does not bond the stem to bone, but it rather fills the gap between prosthesis and bone.
Regarding the implantation technique, a cavity is created into the femur by reaming trabecular bone from inside the medullary canal. Then a bone plug is inserted down into the canal to keep the bone cement from flowing towards the distal femur. When the stem is inserted, the bone cement is pressurized to flow into the trabecular bone. The interlayer (optimal thickness: at least 2 mm) of bone cement – if stable, homogeneous and complete – assures a uniform mechanical load transfer from the implant to the bone. [36] [42] [43]
An inhomogeneous distribution of bone cement may result into implant loosening or into increased risk of periprosthetic fractures. Surgeon must also have experience in preparing the bone cement and respect its polymerization time.
Cemented stems must have a smooth surface, since local peaks of stress must be avoided, as they can lead to cracks in the PMMA layer. Furthermore the stem must be stiff enough to avoid mechanical loading of the cement due to elastic deformation of the metal.

Non-cemented stem

In cementless stems (Fig. 1.14 b), used since 1984 [44, 45], a direct press-fit contact between implant and surrounding bone tissue is realized.
The surgical procedure (Fig. 1.13) includes removal (osteotomy) of the neck and the head of the femur. Once osteotomy has been performed, the cavity for stem's insertion is firstly prepared with an awl and secondly reamed out through a rasp, which has a little smaller dimension than the stem. At this point, a prosthesis of the appropriate size is inserted and driven until it is completely stable. The insertion is carried out by means of hammering blows that need to be carefully controlled in terms of force by the surgeon, since an excessive force, enhanced also by the wedge effect of the stem's shape, may result in a fracture.

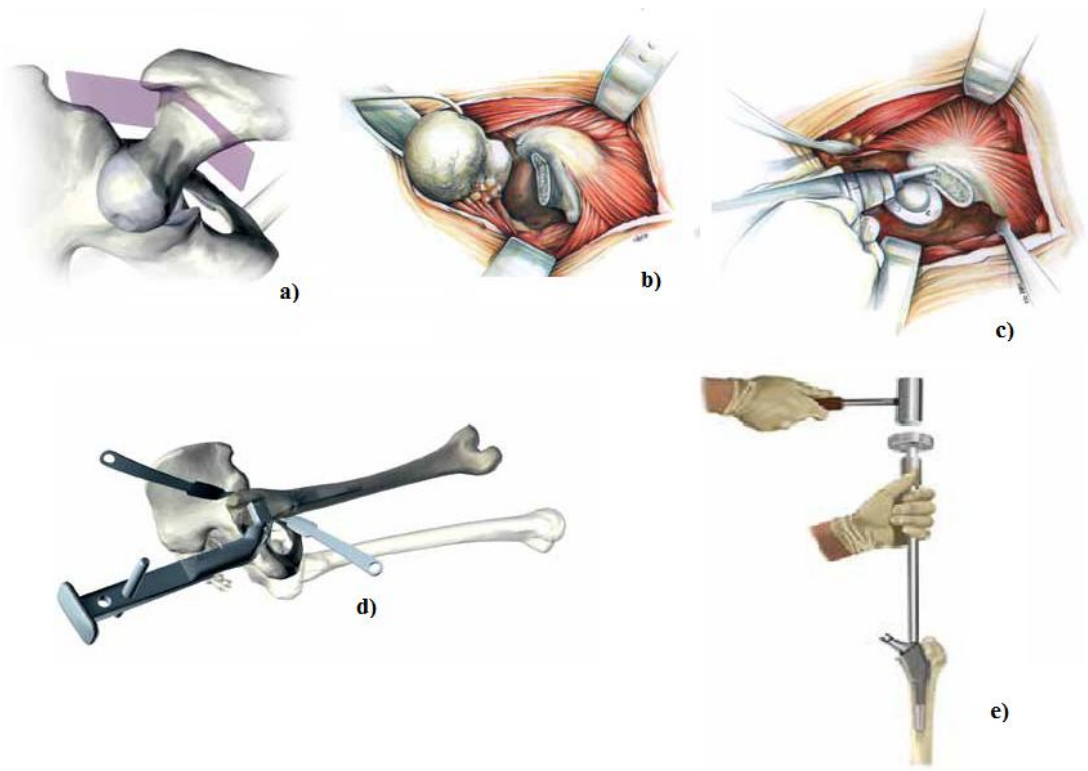

Figure 1.13: Surgical technique to insert cementless stem. Adapted from [46]

a) Resection planes: the lesser trochanter is used as a reference; b) Osteotomy of the femoral neck and head; c) Preparation of the cavity in the medullary canal through the awl; c) The cavity is reamed out with the rasp; d) The stem is hammered down to the cavity until it is stable.

Stability of the stem is basically achieved at two stages: [47]

- *Primary stability:* by hammering the stem into the bone, a geometrical interlocking of the implant is achieved, which guarantees stability in the immediate post-operative period. When the stem is press-fitted, a swelling of the femur's cross-sectional area is observable, causing *assembly strain*. The assembly strain consists of a change in the strain distribution in the bone tissue around the prosthesis. However, if assembly strain is too low, the implant will loosen, if too high bone fracture may occur.
- *Secondary stability:* The bone around the stem that has been damaged during surgery induces a healing response, according to bone remodeling process, which leads the adjacent trabecular bone to grow onto the stem, providing a solid fixation (osseointegration). Moreover, preload condition provided by press-fitting is also helpful for bone growing.

  Long-term osseointegration is further promoted by having either porous coatings or porous surface finish, that are intended to be filled with newly forming trabecular bone.

In the first days post-operatively the patients are prevented from moving, since osseointegration has not begun yet. Later on, progressively increasing loads are applied to the operated hip to foster osseointegration process.

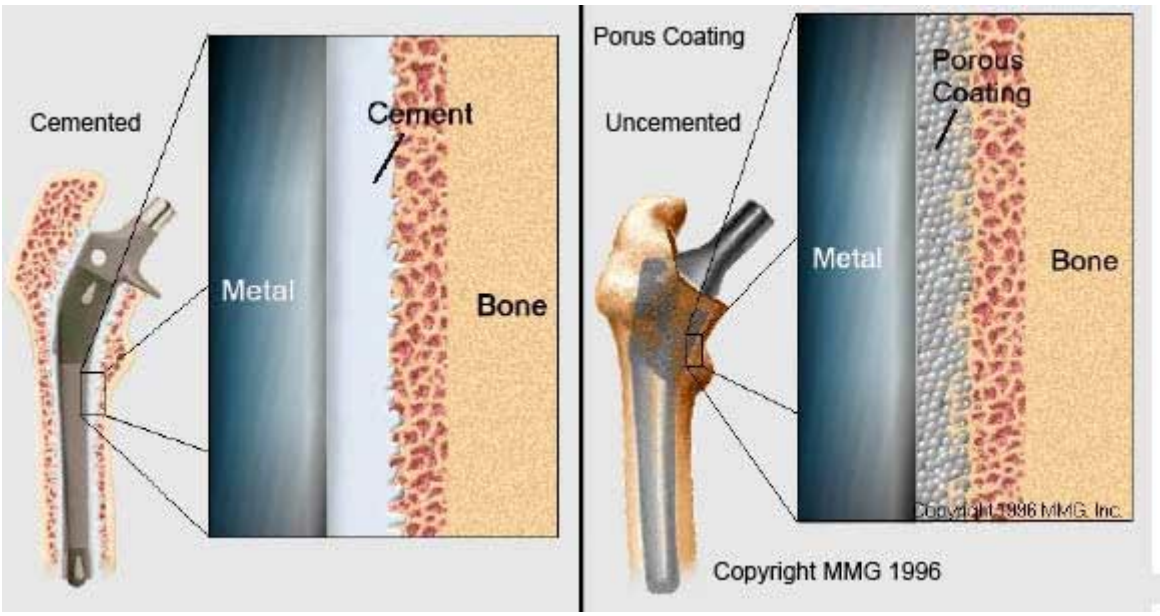

Figure 1.14 : Cemented (a) vs. Non-cemented (b) stems. Retrieved from [48]

The interface bone-implant is highlighted in the picture. Cemented solution (a) considers the use of bone cement that fills the gap between smooth metal stem and the bone. In cementless prostheses, porous coating encourages trabecular bone to grow onto it providing osseointegration

Cemented stem vs. non-cemented stem

Large studies have been carried out to test survival rates and clinical outcomes for both implant solutions [1] [2] [3] and a definitive criterion to prefer one typology rather than the other has not been defined yet [10].

Anyway, some differences have been individuated in literature and the most significant will be highlighted here.

For example, advantages of choosing a cemented stem are a faster rehabilitation for the patient (stability of the stem is almost immediate, due to cement) and less thigh pain [49]. These factors contribute to the fact that cemented stems show higher survival rates in the short- and mid-term. [1] [50]. However, issues connected to bone cement can be sometimes detected: for instance, the unreacted PMMA molecules or the temperature peaks due to the exothermal reaction of polymerization may lead to bone necrosis [35], moreover mechanical deterioration of the cement layer is expected with time due to fatigue.

Furthermore, stress-shielding in periprosthetic femur is more accentuated for cemented stem [24], also because bone cement acts like a bumper between the metal (stiffer, therefore more loaded) and the bone (less stiff, lower loads), shielding the bone from loads and therefore promoting bone resorption. This phenomenon is likely to implicate stem's aseptic loosening, that is one of the major reason running to revision surgery.

Revision surgeries, in terms of removing failed stem and replacing it with a new one, are much easier with cementless stem. In fact, by extracting the cement from the femoral cavity, part of the bone in which PMMA had infiltrated can be removed, implicating a further reduction of bone's quality [51].

Even though cementless implants are more frequently revised because of periprosthetic fracture in the first 2 years post-operatively [2] [52], in long-term period, for younger patients, higher survival rates can be recorded for uncemented stems. [1] [7] [44].

Moreover, porous coating of uncemented stems promotes osseointegration, avoiding stress shielding and depletion of the prosthesis surrounding bone's quality.

However, during the surgical planning phase, clinicians must check bone's quality, since a low bone mineral density or a severe osteoporosis may result in an intra-operative fracture: in fact, the bone may not be able to withstand the forces induced by surgeon's hammer blows.

Therefore, cementless stems are generally more appropriate for younger and more active patients, while for older people is more safe to choose the cemented option, even though individual differences can be vast [8] and other factors, such as muscle quality, gender, bone mineral density, stem design, gait patterns, co-morbidities must be taken into account when choosing the optimal prosthesis [53] [54] [55].

The revision rate for infection is similar for both the uncemented THA and the cemented THA with antibiotic cement. [1]

About rehabilitation times, patients undergoing cemented implants get well faster, while for uncemented prostheses recovery period is extended, since secondary stability must be provided with progressive loads, thus activities must be limited for up to 3 months to protect the replaced hip joint.

1.2.4 Basic Principles of Computed Tomography

Computed Tomography (CT) is a medical imaging technique, providing slice images of the body, that allows to distinguish different organs and tissues depending on their density.

A motorized table moves the patient through a circular opening (gantry) in the CT machine. As the patient passes through the CT imaging system, an X-ray tube generator rotates around the inside of the circular opening. (Fig. 1.15)
The X-ray source produces a beam used to irradiate a section of the patient's body. The radiation that is not absorbed by the tissues is measured by a system of detectors integral with the source: in this way it is possible to record a series of X-ray attenuation profiles of the patient's scanned body.
Many different “snapshots” (angles) are collected during one complete rotation.
Afterwards, the data are sent to a computer, which through complex algorithms is able to reconstruct all of the individual "snapshots" into a cross-sectional image (slice) of the internal organs and tissues for each complete rotation of the X-ray source.

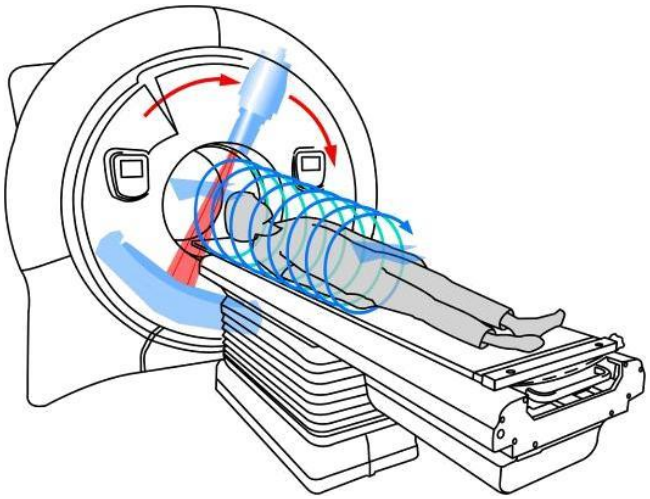

Figure 1.15: Illustration of Helical Tomography delivery

Each slice of the body is divided into elementary volume units (voxels). The number of voxels depends on detectors' number and dimensions.
Knowing the difference between the emitted intensity (I_0) and the detected intensity (I_n), a CT number is assigned to every voxel. The CT number of a given voxel is the average value of all the linear attenuation coefficients of the beam-crossed tissues considered in the volume and indicates how much energy of the X-ray beam is reduced by passing through these tissues. Attenuation coefficients refer to Lambert-Beer's law of radiant energy's attenuation (Equation 1.1):

$$I_n = I_0 e^{-(w_1\mu_1)} e^{-(w_2\mu_2)} \dots e^{-(w_n\mu_n)} \qquad [1.1]$$

given $i = 1,2, \dots, n$ as voxels along the path of a ray, w_i as the path length of the ray through i-th voxel and μ_i as the attenuation coefficient of the material contained within i-th voxel. (Fig. 1.16)

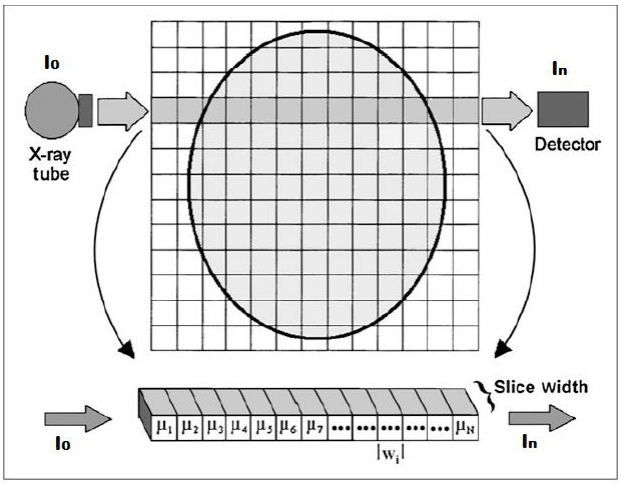

Figure 1.16 : Scheme of the attenuation principle

Every tissue has its own linear attenuation coefficient, but since these coefficients can vary due to different CT scan models and different settings on the same scanner, the Hounsfield Unit scale is used to standardize them. [56] [57] [58]

The HU is defined as described in Formula 1.2:

$$HU = \left(\frac{\mu_X - \mu_{Water}}{\mu_{Water} - \mu_{Air}}\right) \times 1000 \qquad [1.2]$$

where μ_X is the average attenuation coefficient of the voxel, while μ_{Water} and μ_{Air} ($\mu_{Air} \approx 0$) are the linear attenuation coefficient of water and air. Conventionally, at standard pressure and temperature conditions, water is set to 0 HU and air to -1000 HU.

Each voxel with its CT number (i.e. HU) will be represented in a gray values scale.
Since attenuation depends on the density of the scanned volume, different levels of gray lead to distinguish between soft and hard tissues.
Moreover, by calibrating the CT scanner with a phantom it is possible to define the relationship between HU and BMD, as it will be analyzed in § 2.2.3 .

A single voxel may contain of several types of tissues due to the finite spatial resolution of the imaging device. This phenomenon, termed partial volume effect (PVE), complicates the segmentation process. For example, at the interface between a softer and a harder tissue (i.e. outer cortical bone or internal interface between metal stem and bone) the edge may appear as blurred.

1.3 Aim of the Thesis

Measuring bone mineral density in vivo provides quantitative information on bone's quality, that can be used for several applications. For instance, with regard to THR, bone densitometry can be used to predict femoral strength [59]; moreover, it provides useful information about bone architecture around implants and its change over time [60] [61].
There are different techniques to measure bone mineral density: plain radiographic absorptiometry, dual energy X-ray absorptiometry (DEXA) and quantitative computed tomography (CT).
Quantitative CT is the most accurate and reproducible method for in vivo evaluation of cortical and cancellous bone density, [62] [63] and is the only technology that allows a three-dimensional volumetric analysis, since it provides a stack of cross-sectional images.

However, patients undergo higher radiation dose if compared to DEXA (0.5-1.0 mSv against 0.001-0.1 mSv). [62]
Application of bone densitometry based on CT are multiple: assessment of volumetric BMD is indeed the basis for generating and developing subject-specific FE models both to estimate mechanical structural behavior of the bone-implant system [64] and to predict bone remodeling and stress shielding around the prosthesis. [63] [65] [66] [67]

In this study, bone densitometry measurements through CT are used for novel subject-specific methods i) to assess the intra-operative risk of fracture (based on FEA) and ii) to evaluate changes in BMD, by comparing post 24h and post 1y data.

1.3.1 Fracture Risk Assessment

The purpose of this part of the study is to develop a novel in silico subject-specific method to evaluate the risk of periprosthetic fracture when the surgeon hammers the cementless stem down to the femoral cavity.
The evaluation of the fracture risk is carried out by generating a 3D model, that is successively discretized and used for a FE mechanical structural analysis. The 3D model is built thanks to BMD measurements from CT images.
Other aim is to locate which part of the bone is more likely to fail.
This work is based on the previous models [10] [53] [55] developed in the frame of the aforementioned project “Clinical evaluation score for Total Hip Arthroplasty planning and post-operative assessment”.
This method aims to be a development of the previous FR assessment models since it takes into account different external factors in the FE analysis. This means that different boundary conditions, in terms of loads, are here considered in order to answer to the demand of more robustness [53]. In fact, the novelty of this method is taking into account factors like material roughness, tapering degree, cross-sectional area and friction at the bone-implant interface.
Moreover, in prior works various failure criteria have been used for FR assessment, such as Von Mises equivalent stress [53]. However, it has been demonstrated that a failure criteria based on maximum principal strains is a suitable candidate for the in vivo risk assessments. [68]

By processing 5 patients, this study also wants to test the feasibility and repeatability of the methodology in order to suggest a future use in the clinical evaluation score for pre-operative implant decision making.

1.3.2 Bone Mineral Density Changes

According to the follow-up protocol developed by Landspitali – University Hospital of Iceland and University of Reykjavik, patients undergo 2 CT-scans 24 hours and 1 year after total hip arthroplasty.
Based on BMD measurements by means of these two CTs, this study's aim is to assess mineral density changes of the femoral bone in 1 year time span after the surgery.
Checking how BMD has increased/decreased around the prosthesis is a useful tool to estimate bone's remodeling.
Differently to DEXA, CT-scan allows to have a three-dimensional measure of the bone mineral density. As suggested in other works too [69], by using the image processing software Mimics, it was possible to exploit this powerful feature and to develop a new protocol for the evaluation of the three-dimensional changes of BMD.
The novelty of this method lies in the opportunity to quantify volumetric bone growth/loss and to visually localize its three-dimensional distribution.
5 patients' data are processed with this method, in order to investigate the potential of quantitative CT volumetric analysis to quantify bone changes after THR and verify its feasibility and repeatability.
The same 5 patients have been also processed with an alternative method, developed in parallel at ETH – Zürich [70] which uses open source image processing software – instead of Mimics – and a more automated image registration technique. The results have been compared for a cross-checking validation and to determine advantages and disadvantages of each method.

2. Materials and Methods

2.1. Study Workflow

Figure 2.1 shows a scheme representing the overall workflow for both the assessment of the intraoperative FRI and the evaluation of the BMD changes occurring in the periprosthetic area of the femur one year after total hip arthroplasty.

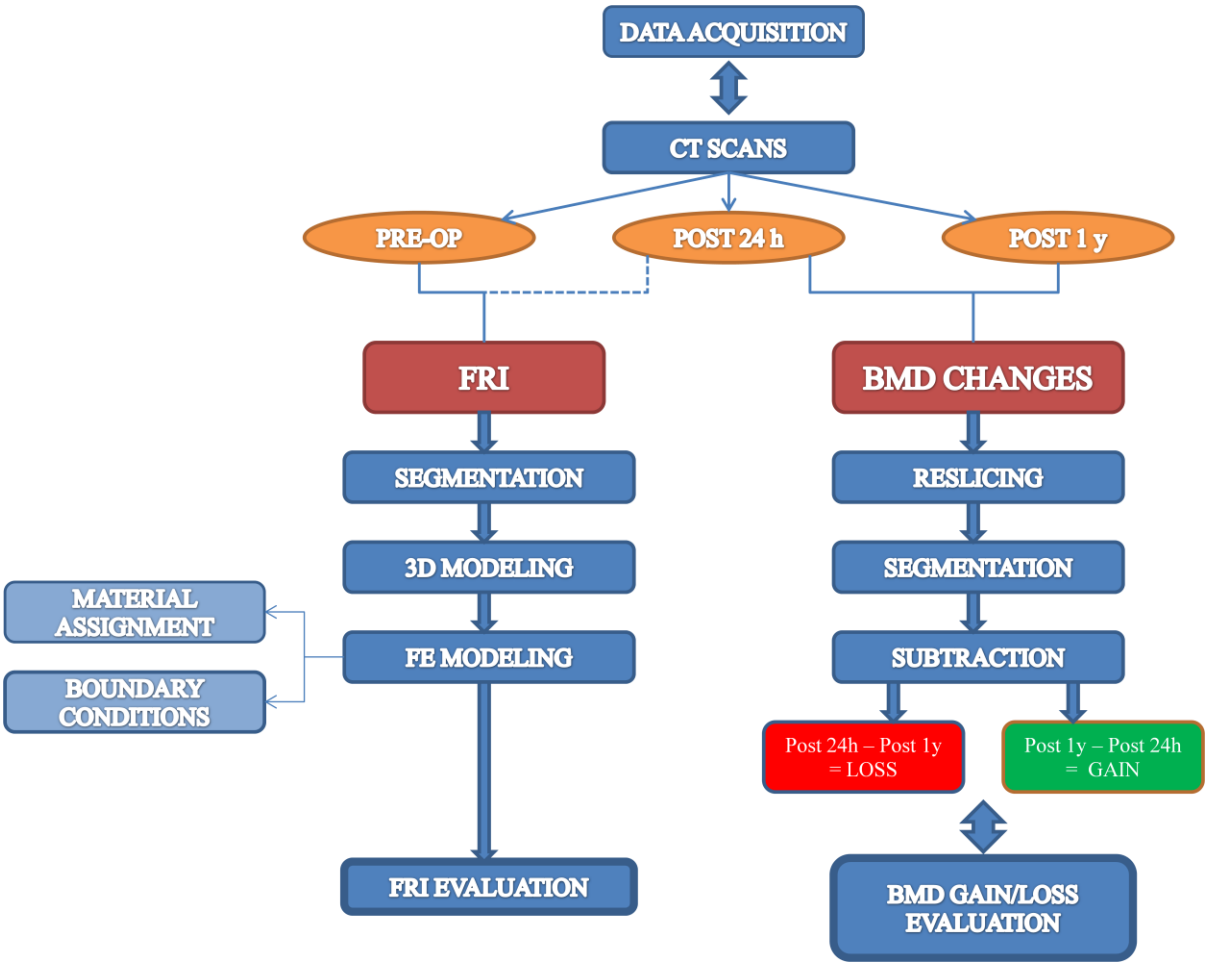

Figure 2.1: Study Workflow

First step is to gather all the CT-scans of the selected patient. For each patient three CT-scan datasets are provided by the University Hospital of Iceland – Landspitali: one of them was carried out pre-operatively, the other two were done 24 hours and 1 year post-operatively.

To estimate FRI during the implant hammering operation, pre-op CT-Scan is mainly considered, having the post 24h one as a reference for the 3D model. Working on pre-op CT

images, a segmentation is carried out to isolate the interesting areas for the successive creation of the bone's 3D model.
Successively, the 3D model is discretized with a finite elements mesh. Material properties of the bone are assigned basing on HU values.
Later on, boundary conditions are defined and the strain distribution within the FE model of the femur is calculated in order to assess the FRI.

For the evaluation of BMD changes in the operated proximal femur one year post-operatively, a comparison between post 24h and post 1y CT-scans was made.
Firstly, a reslicing of both the original CT images datasets is done. Next step is to segment the bone, thereafter the two CT images datasets are registered using the subtraction fusion method. It is necessary to make the registration + subtraction operation twice, since BMD gain and loss are evaluated separately: subtracting post 1y dataset from post 24h one leads to assess the BMD increase, while subtracting post 24h from post 1y gives the BMD decrease.

2.2. Data Acquisition

2.2.1. Subjects Information

The two present methods developed to evaluate the intraoperative FRI and the BMD changes were applied to patients that have already joined up the "Clinical evaluation score for Total Hip Arthroplasty planning and post-operative assessment" project, born from the collaboration between the University of Reykjavik and Landspitali – University Hospital of Iceland. The whole cohort of the project enumerates patients undergoing primary THA surgery (unilateral arthroplasty), and considers subjects having both cemented and cementless stems.
Nevertheless, for the purpose of this study, a total of 5 patients (3 males plus 2 females) having cementless implants has been selected from the whole project cohort. The youngest patient was 19 years old at the time of the first CT, while the oldest one was 60. The average age is 46.0 ± 16.8 years.

All the information about patients' gender, age and operated side are summarized in the Table 2.1.

Patient's no.	Age	Sex	Type of Implant	Operated Side
1	50	M	Uncemented	L
2	42	M	Uncemented	L
3	60	F	Uncemented	L
4	59	F	Uncemented	R
5	19	M	Uncemented	R

Table 2.1 : Subjects' Info

2.2.2. CT Acquisition

The patients are scanned with a *Philips Brilliance 64 Spiral-CT* machine (Fig. 2.2) three times in one year: firstly 1-3 days before surgery and successively 24 hours and 52 weeks after surgery.
The CT scanning region extends from the iliac crest to the middle of the diaphysial femur.

Slices thickness is 1 mm, slice increment is 0.5 mm and tube voltage is set to 120 kVp. Every slice has 512x512 pixels; each pixel is represented by a GV belonging to a 12-bit representation scale (4096 different levels of gray). Each GV has a corresponding value in the HU scale, following the relation:

$$[GV] = 1000 + [HU]$$

This imaging protocol allows an accurate 3D reconstruction of the proximal femur.

Figure 2.2: Philips' Brilliance 64-slice CT scanner

The CT images acquired after the THA are corrupted from metal artifacts that introduce both bright and dark streaks which modify remarkably HU values and therefore bone and muscle density. (Fig. 2.3)

For this reason, post 24h and post 1y CT images are processed in the artifact reduction software *Metal Deletion Technique* from ReVision Radiology [71]. By means of this software artifacts are iteratively reduced and the "clean" image reconstructed, thus the BMD assessments explained in this paper can be performed.

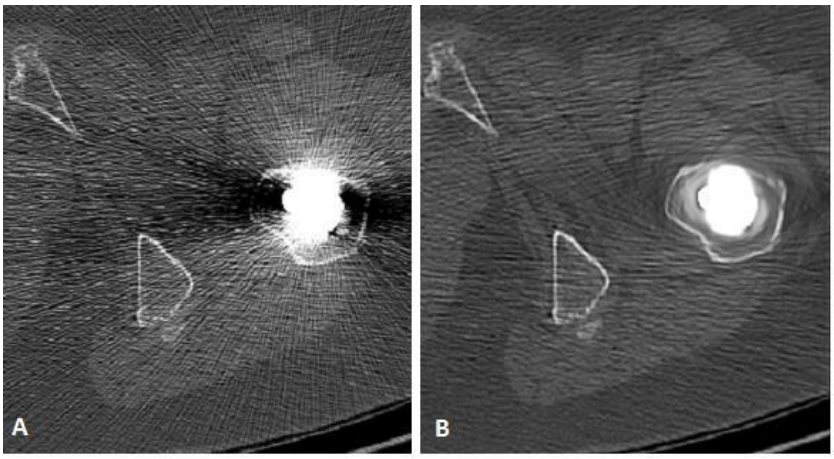

Figure 2.3: A) CT-slice of a post-op THR, with artifacts due to the metallic stem. B) The same CT-slice after artifact reduction: no streaks are now present. [10]

2.2.3. CT Calibration

Prior to the study, the CT-Scan device was calibrated [72] using a QUASAR™ Phantom in order to find a mathematical relationship that allows to convert the CT-Scan values (in [HU]) into apparent density, i.e. BMD (in [g/cm³]).

The resulting formula [2.1] is:

$$BMD\ \left[\frac{g}{cm^3}\right] = 0.000902\ HU + 0.0419 \qquad [2.1]$$

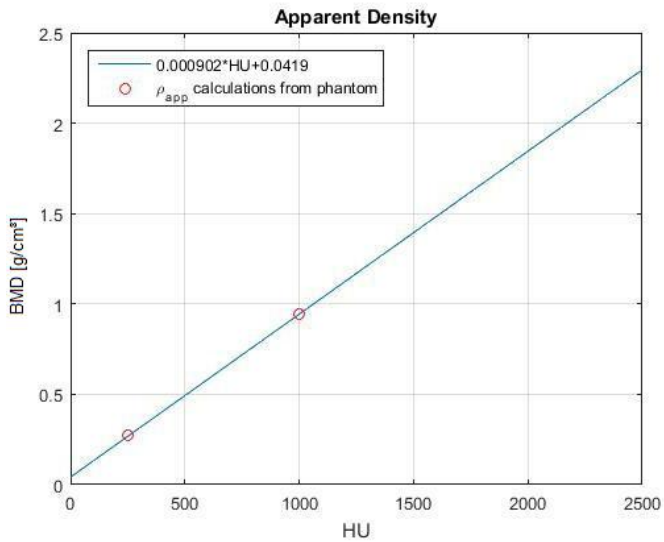

Figure 2.4 : BMD vs. HU relationship

For example: 1000 HU (cortical bone) correspond to an apparent density of 0.94 g/cm³

2.3. Fracture Risk Index

The novel subject-specific method to assess the fracture risk of the periprosthetic area of the proximal femur is described in the following sections. This method was applied to evaluate the FR for all the 5 patients enrolled in this study.

2.3.1. Segmentation

Firstly, Pre-op CT-Scan images (available in DICOM format) are imported into the software Materialise Mimics®.
There, in order to take into account just the part of the image corresponding to the proximal femur, a segmentation is carried out. By using the 3D Live Wire Mimics' tool, the contour of the bone is traced and all the pixels belonging to the femur are gathered into the same coloured mask. (Fig. 2.5 a)

2.3.2. 3D Modeling

Once the mask has been created, a three-dimensional model of the pre-op femur is generated. The 3D bone has still got the neck and head: it is necessary to cut them off since they are removed in the first steps of the surgical operation theatre.
To simulate this osteotomy, the 3D model of post-surgery femur (created from post 24h CT-scan) is imported in the pre-op Mimics project.
Using the Reposition tool, the 3D post-op femur is manually dragged and rotated within the pre-op spatial reference system, as long as the 3D post 24h femur overlaps the pre-op one. Once reposition has been performed, the mask of the post 24h bone is obtained from the 3D model, through a tool available in Mimics.
Successively, two Boolean subtractions are carried out. First of them is performed between the just-created masks: by subtracting post 24 h mask from pre-op one, a "scrap mask" is obtained. Secondly, by doing pre-op mask minus scrap mask it is possible to get the mask of the femur ready for the prosthesis insertion. (Fig. 2.5 b and Fig. 2.5 c). Next step is to generate the 3D model from the latter mask.

This 3D model is devoid of the neck and the head, and has got the cavity for the stem; moreover, since it has been generated inside the pre-op Mimics file, there are no metal artifacts, that have an adverse effect on proper material assignment for the FE model, which is HU-based, as it will be discussed further.

Additionally, a virtual distal cut is performed orthogonal to the femur's long axis, about 2 cm below stem's tip.

Finally, the hollow 3D femur is improved with some refinements, such as Wrapping and Smoothing – tools available in Mimics – to avoid sharp edges (Fig. 2.5 d).

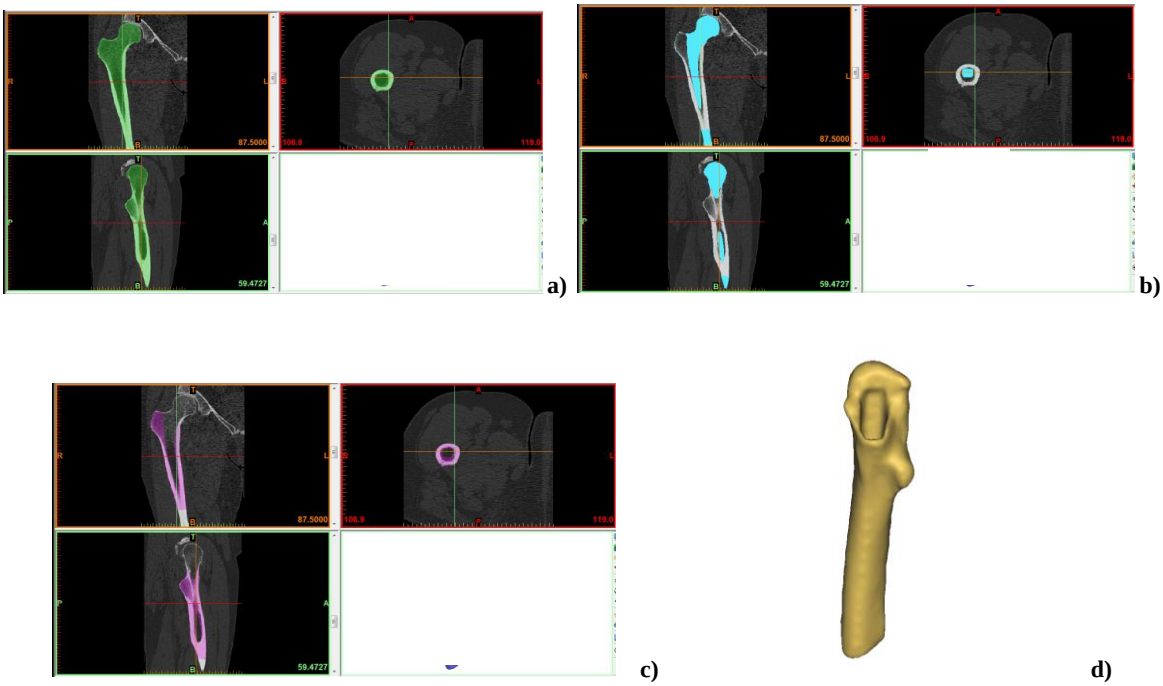

Figure 2.5 : Steps to create the 3D model

a) Pre-op femur mask ; b) Scrap mask; c) Femur_with_cavity mask; d) 3D model

2.3.3. FE Modeling

The final 3D femur is exported into 3-Matic in order to discretize its volume through a finite element mesh.

First step is to create a surface mesh of triangular elements with automatic Remesh tool, setting the maximum edge length and checking the shape quality to avoid too distorted elements through mesh-refining tools available in 3-Matic. To do that, a value of 0.3 has been set as the lowest threshold for the shape quality criterion R-in/R-out; moreover, 0.05 has been

defined to be the maximum geometrical error, which is the maximum deviation between the part's surface before and after automatic remeshing operation.

Later on, the volume mesh is generated starting from the surface, using 10-nodes tetrahedral structural solid elements (SOLID187). (Fig. 2.7)

Quality has been checked also for the volume mesh, meaning that before implementing the volume-meshing automatic algorithm, the lower-threshold Aspect Ratio value has been set to 25.

The choice of the optimal elements' maximum edge length (i.e. the proper mesh density) has been made following the results of a convergence test. Since smaller element's dimension means larger number of nodes and elements, the average maximum principal elastic strain over a sample area has been calculated to determine the proper mesh density for different maximum edge lengths of the elements. For the convergence test the same boundary conditions as for FR assessment have been set.

The outer lesser trochanter zone is the selected sample area.

Table and plot below show the result of the convergence test:

Maximum edge length	**Number of Elements**	**Number of Nodes**	**Average Max Princ El Strain in Lesser Trochanter**	**Error** (compared to previous size result)
8 mm	38916	67745	763 με	-
5 mm	55667	89826	1150 με	51%
4 mm	85515	129734	1450 με	26%
3 mm	176372	252111	952 με	34%
2,5 mm	295778	413365	1080 με	13%
2 mm	567491	779603	License not available	-

Table 2.2 : Convergence Test results

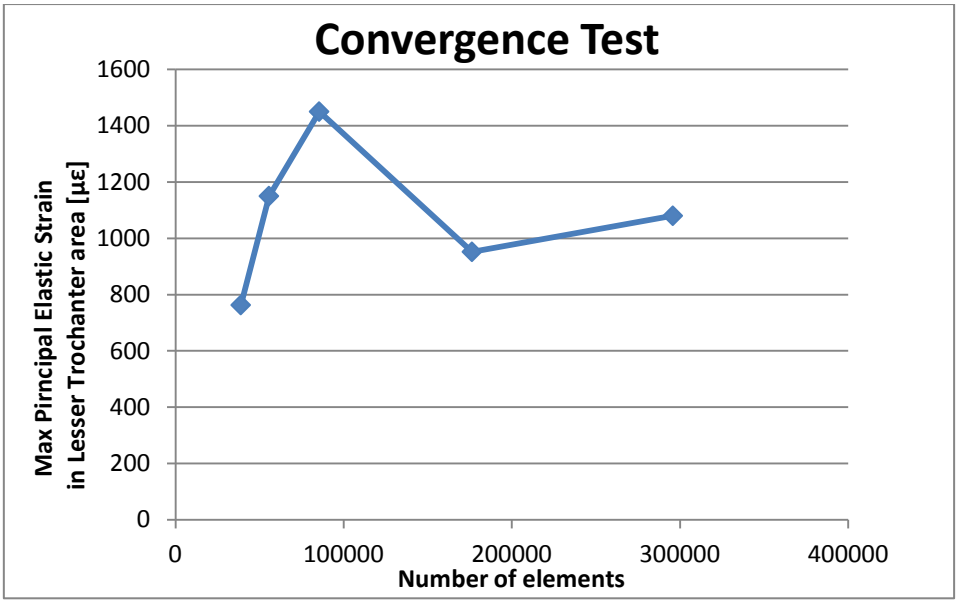

Figure 2.6 : Convergence Test

A mesh edge size of 2.5 mm was selected since the difference between results obtained with 2.5 and 3 mm sizes is small if compared to the others; therefore a certain convergence is supposable if increasing the number of elements. Unfortunately, software license has not allowed a further increasing of elements number, and 2.5 mm is the smallest usable size. Moreover, the choice of the smallest size is justified by the fact that the smaller is the element, the lesser number of voxels are counted in a single element, and this allows a more detailed material assignment. In fact, Mimics firstly averages on each element the HU field and then, through mathematical relationships, derives the element Young's modulus as it will be explained in the next paragraph.

Smaller elements mean higher computational cost in terms of elapsed time for processing, though.

Figure 2.7 : Volume mesh of the femur model

2.3.3.1. Material Assignment

Once the volume has been discretized, the FE model is imported back to Mimics in order to assign mechanical material properties to the bone, which are substantially based on the average HU of each finite element (see Formula [2.1]).
For simplification, in this method, each finite element has been considered as locally linear-elastic and isotropic.
The inhomogeneity of the bone has been also simplified by defining 50 different materials to be assigned to the bone mesh: this means that elements having similar HU values are "made of" the same material. An apparent density, a Young's modulus and a Poisson's ratio are defined for each material.
The apparent density (ρ_{app}) is defined according to the above-mentioned HU-BMD conversion formula [2.1].
The relationship between ρ_{app} (in [g/cm3]) and Young's modulus is described by the equation retrieved from [73]:

$$E[\text{MPa}] = 6850\ {\rho_{app}}^{1.49} \qquad [2.2]$$

Equation 2.2 has been used to both represent trabecular and cortical bone.
Finally, the same Poisson's ratio equals to 0.3 has been set for all the materials.

The mask of the femur – from which the 3D model is generated – may contain pixels with a very low HU: this means that those image elements belong either to soft tissues, bone marrow or air bubbles. For the continuity of the FE model it is necessary to keep also these entities, that are mainly in the inner part of the bone, even though they are not structural elements and they contribute to underestimate the bone strength. Moreover, if these elements have negative HU (in particular < -35 HU), according to formulas [2.1] and [2.2], a negative Young's modulus would be expected, which is unrealistic.
To overcome this issue, the same "weaker" material is assigned to all of the finite elements having a corresponding apparent density lower than 0.01 g/cm^3.
Thus, the fictitious material has been defined to have a ρ_{app} = 0.01 g/cm^3, that (according to [2.2]) leads to E = 7 MPa, which is 2 order of magnitude smaller than the lowest-density bone (255 HU, ρ_{app} = 0.27 g/cm^3 and E = 984 MPa).
The Poisson's ratio for this material is still 0.3 .

Figure 2.8 and 2.9 shows the distribution of the assigned materials throughout the bone.

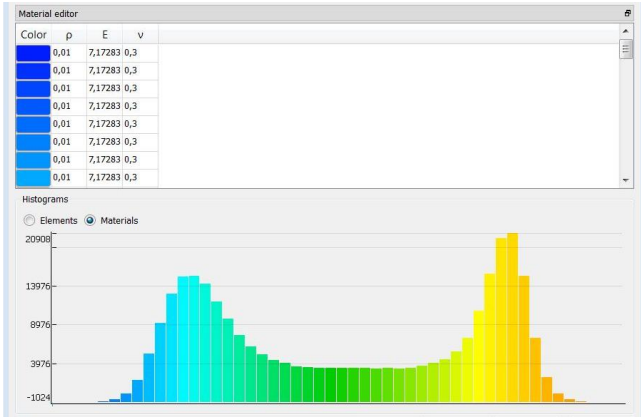

Figure 2.8 : Materials Histogram

Yellow/orange elements have the highest HU i.e. the highest ρ_{app} and E

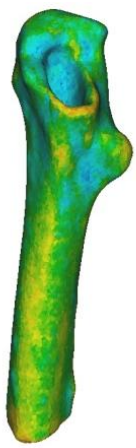

Figure 2.9 : Material Distribution

2.3.3.2. Boundary Conditions

The three-dimensional FE model of the proximal femur is imported into Ansys Workbench in order to perform the mechanical simulation to assess bone's behavior consequent to the press-fitting of the non-cemented stem.

Within Ansys Workbench environment, the Finite Element Modeler and the Static Structural modules have been used to carry out the computational simulation.

Firstly, a constraint and an external load (boundary conditions) have been defined. Similarly to previous models [53], a fixed support is determined by selecting a ≈ 2 cm high portion of the most distal part of the femur's model, right below the stem's tip (Fig. 2.10 a). This constraint allows an analysis of the strain distribution (as it will be further discussed) just around the periprosthetic area, trying to minimize the bending moment of the femur's shaft and avoiding any distal displacement.

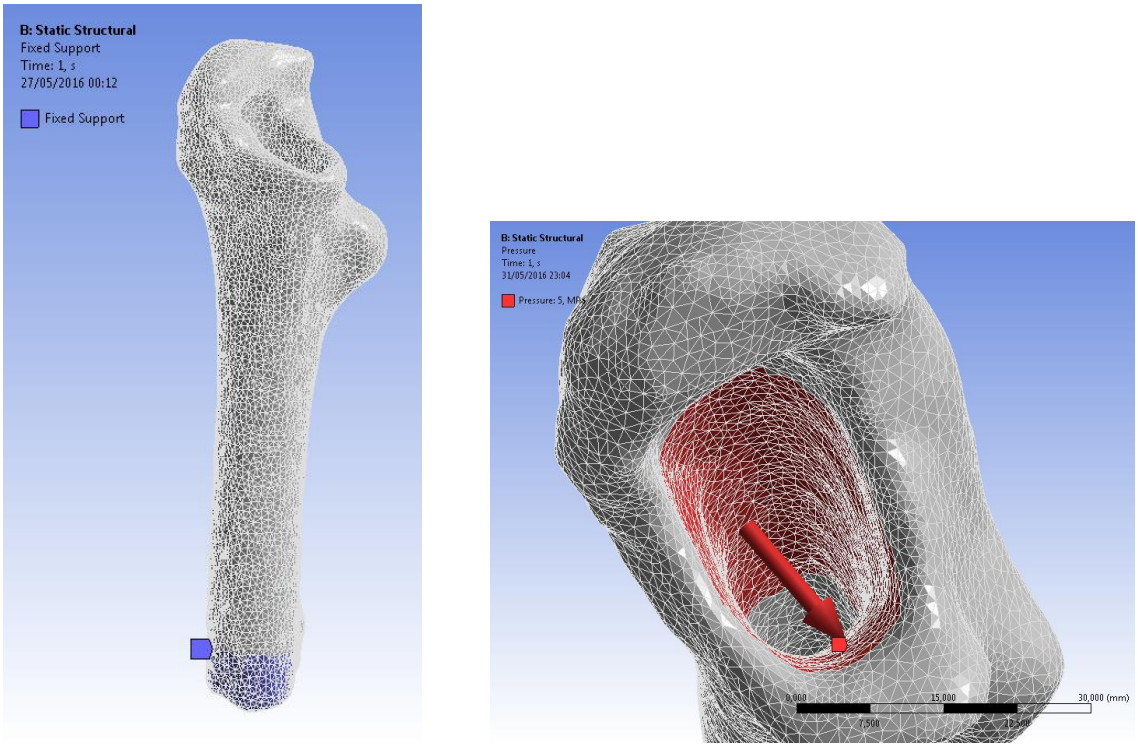

Figure 2.10 : Boundary Conditions

a) Fixed Support; b) Applied Pressure

In the state of the art [9] [53] [55] the external loads are two equals and opposite forces applied in two small areas in the medial and lateral side of the femoral cavity. (Fig.2.11)

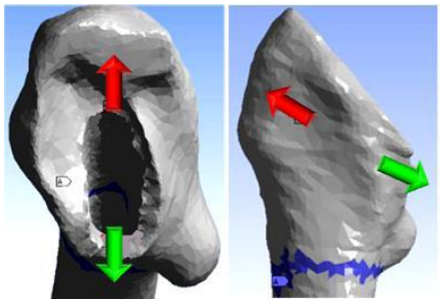

Figure 2.11 : External loads directions in previous model [53]

Thus, this approach means that the same load is applied to all the patient, not considering some factors that can significantly contribute to differentiate the bone's response to the press-fit, depending on the patient.
This novel method includes factors such as stem design, material roughness, tapering degree, cross-sectional area and friction between bone and stem surfaces, aiming to respond to the lack of robustness of previous methods. All these variables directly influence the external load's magnitude, which is not a concentrated force anymore, but a uniform pressure, to be applied on the proximal inner surface of the cavity (Fig. 2.10 b).

Theory behind this method considers the bone-stem system modeled as a conic coupling. [74] [75]
Dynamics of the cementless stem being hammered into the femur can be understood starting by considering the collision between two rigid bodies (hammer and stem). Every single hammer blow to the implant can be viewed as two discrete events: in the first one the implant is accelerated due to the impact, in the second one the implant moves within the bone, where it is decelerated until it stops.
During the impact a large force is exerted to the stem over a very short time, this force can be expressed according to Newton's second law of motion:

$$\boldsymbol{F} = \frac{d\boldsymbol{p}}{dt} = m\,\frac{d\boldsymbol{v}}{dt} \qquad [2.3]$$

having the force F [N], the momentum p [kg m/s], the mass of the implant m [kg] (here reasonably considered as constant) and the velocity v [m/s]. A large peak force is achieved in a very short time that can be on the order of microseconds. Thus, according to [2.3] the implant is accelerated by the impact.
Now, let's consider the model (without damping terms) for the dynamics of the implant insertion into a femur, schematized in Fig. 2.12:

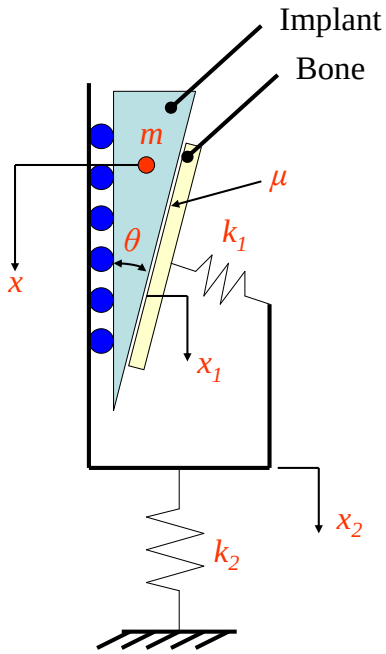

Figure 2.12 : Dynamic model of implant insertion [74]

k_1 represents the increase in preload force between the bone and the implant while the stem is driven deeper into the femur; k_2 describes the axial and shear compliance of the bone. Friction factor between stem and the bone is μ. x_1 is the displacement of the implant in respect to the bone, while x_2 is the displacement of the implant in respect to the ground as result of system's compliance only. The total displacement in the fixed reference system (the ground) is x, having $x = x_1+x_2$.

Firstly, the implant starts to move into the bone and the k_2 spring absorbs kinetic energy from the implant. In this phase dynamics of the implant is described by equation 2.4:

$$m\frac{d^2x}{dt^2} = k_2x_2 \qquad [2.4]$$

At a certain time, the elastic reaction force of k_2 spring exceeds the sticking limit between the bone and the stem causing the implant to slip. During the slip, kinetic energy is dissipated in the friction. The slip conditions is represented by equation 2.5:

$$m\frac{d^2x}{dt^2} > k_1x_1 \sin\theta\,(\sin\theta + \mu\cos\theta) \qquad [2.5]$$

Thus, every single hammer blow two different situations happen, as shown in Fig. 2.13:

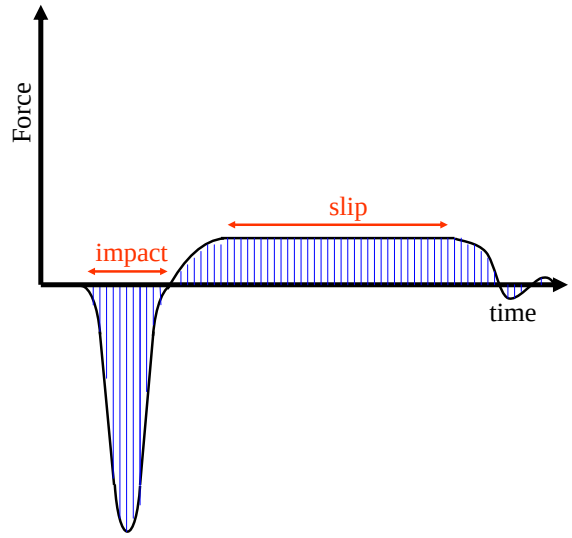

Figure 2.13 : Force over time profile of the implant being hit by one hammer blow [74]

First peak represents the impact between the hammer and the stem that leads to acceleration of the implant. The second phase corresponds to the sliding phase, in which kinetic energy is dissipated by friction between bone-metal and the implant is decelerated. At the end, it may be possible to record oscillation of the implant.

After each blow of the surgical hammer, the implant is driven farther into the cavity, compressing k_1 and progressively increasing the frictional force. At a the n-th hammer blow frictional force will overcome the reaction force from k_2 and the implant will stop slipping, being in a firm contact with the bone. The maximum force exerted on the implant is F_{max}, and it corresponds to no slip. (Fig. 2.14). In the rest of the paper, the notation F_e (external force) will be used, bearing in mind that it refers to the F_{max}.

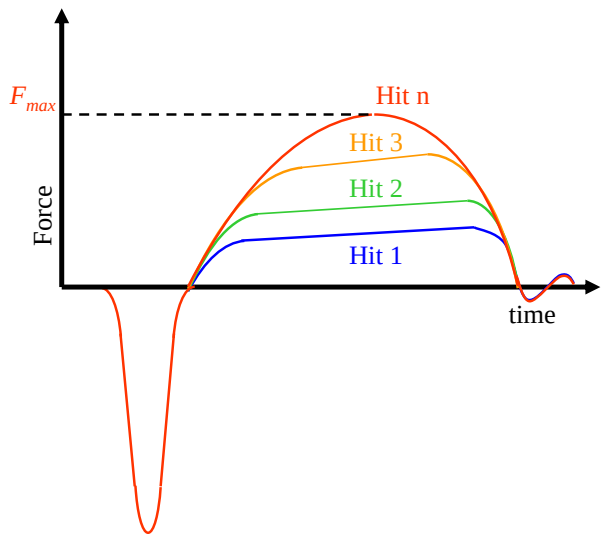

Figure 2.14 : Trend of the force over time on the implant after n hammer blows [74]

To analyze the forces exerted from the implant to the bone, scheme in Fig. 2.15 a) must be considered. Here, the bone-implant system is assumed – with a certain level of approximation – as a conic coupling, [75] where the stem is press-fitted into the cavity of the femur.

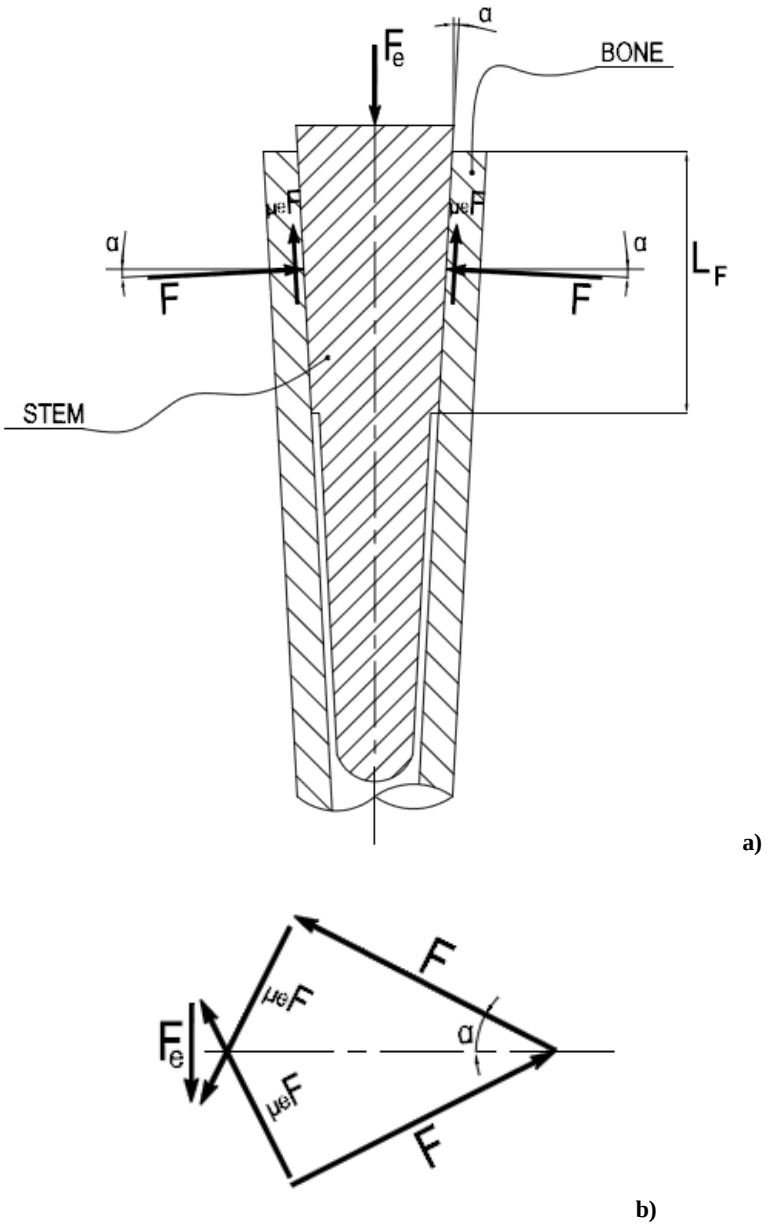

Figure 2.15 : a) Model of the bone-stem conic coupling with forces involved in the system.
b) Forces polygon for the equilibrium

As already seen, F_e is the maximum force exerted on the implant, accumulated after the last surgeon's hammer blow and corresponding to no slip of the same.
The implantation force, due to the wedge effect of the conic shape (taper angle is α) , generates the two pressing forces F. Furthermore, frictional forces arise because of the contact between the stem and the bone tissue, and they are characterized by the interference coefficient μ_e.
Considering the polygon to determine forces equilibrium (Fig. 2.15 b), equation 2.6 expressing F_e is obtained:

$$F_e = 2\,F\ \cos\alpha\,(\tan\alpha + \mu_e) \qquad [2.6]$$

To calculate the coupling pressure, the cone can be considered as a press-fitted cylinder, long L_F , that has a perimeter equals to the average between the top cross-sectional and the bottom cross-sectional areas of the stem. This average perimeter is indicated as per_m.
Thus, forces F exerted on the bone are related to the coupling pressure p according to equation 2.7:

$$2\,F = p\,per_m L_F \qquad [2.7]$$

Inserting equation 2.7 in equation 2.6 and manipulating it, it is possible to find the relationship between the external implantation force and the pressure that will result because of the interference fit. This relationship is expressed by equation 2.8:

$$p = \frac{F_e}{per_m * L_F * \cos\alpha\,(\tan\alpha + \mu_e)} \qquad [2.8]$$

With regard to the load condition of the FE model, the pressure p is uniformly applied on the proximal inner surface of the cavity (Fig. 2.10 b).
Hereunder, factors that influence the magnitude of the applied pressure are analyzed in detail:

- F_e is the maximum force exerted on the implant, accumulated after the last surgeon's hammer blow and corresponding to no slip of the same. Its value has been set to be 9250 N, as measured in a prior study [76].
- L_F is the length of the conic coupling, that is to say the height of the conic cavity's lateral surface where pressure has to be applied. L_F is estimated to be 45% of the stem's length L, starting L_F measurement from the top of the

calcar area (Fig. 2.16).Through Measurement tool in Mimics, parameter L is acquired from Post 24h CT, where the stem is present.

In addition, for instance, the assumption made about region of contact can be confirmed by looking at the design of the rasps used by surgeons for reaming, made for Zimmer CLS® Spotorno® stem (Appendix A-1), which is widely used in THAs performed at Landspítali – University Hospital of Iceland.

Rasps present zone II and zone III which are used to prepare both cancellous and cortical bone to the contact with the stem by means of its cutting edges (Fig. 2.17). Thus, for all the patient, basing on the size of the stem (i.e. L), the parameter L_F is determined.

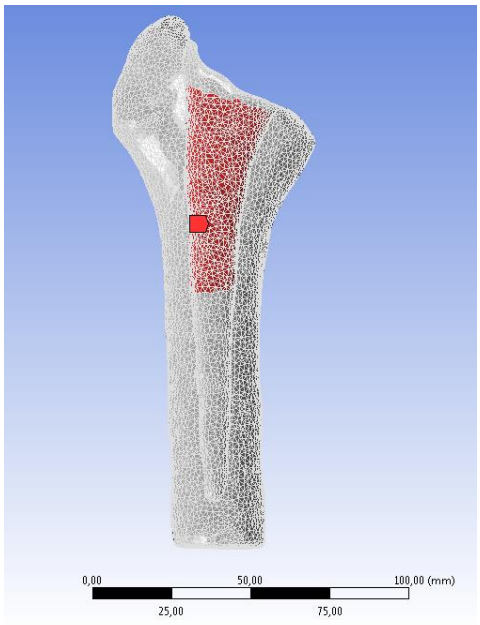

Figure 2.16 : Clipped view of the meshed femur

Relevant contact area is enlightened in red, whose height is Lf

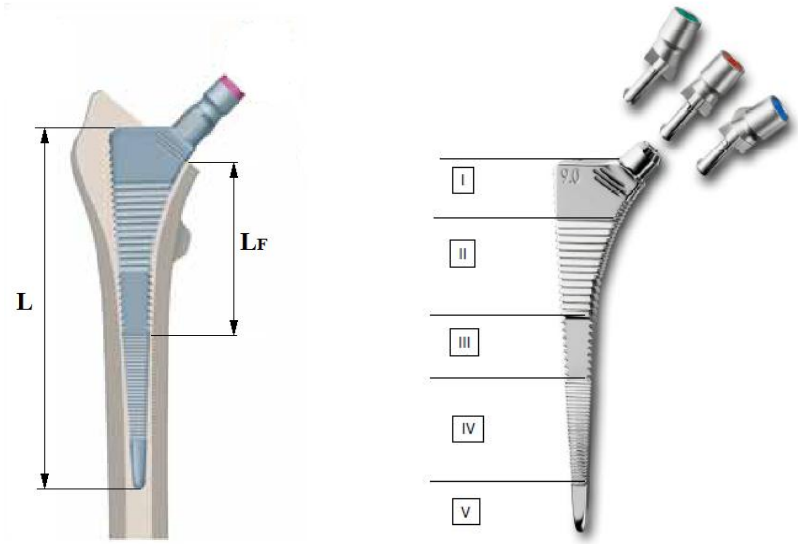

Figure 2.17 : Lf referring to Zimmer® rasp

- α is the taper angle of the stem. Real cementless stems generally have a three-dimensional tapering shape; nevertheless, in this study, the stem has been simplified to be conical, with an angle of inclination of 2.5°, using the model developed in [77].
- μ_e is the interference coefficient of implant insertion, and represents the dynamic friction between the spongy bone and the stem. From a previous study [78], μ_e has been defined to be between 0.44 (higher test loads) and 0.54 (lower test loads), for titanium alloy stems having a Al_2O_3 blasted surface with surface rugosity of R_a = 11 μm. Considering, for instance, Zimmer CLS Spotorno® stem (Appendix A-1), whose surface rugosity reaches R_a = 4÷6 μm, and considering that load in this model is higher than in [78], it is reasonable to assume μ_e = 0.4 .
- per_m is the average perimeter of the cavity, if considering just the relevant contact area, whose length has been already defined to be L_F.

  per_m is the other subject-specific parameter (in addition to L_F), as it depends on the size of the cavity for the stem (and therefore the stem itself), that is related to femur's dimension. In this method, per_m is evaluated using the Measurement tools in Mimics, by calculating the average between the perimeter of the cavity in the most proximal axial slice (Fig. 2.18 a) and the perimeter of the cavity in the most distal axial slice of the contact area (Fig. 2.18 b), both considered in the axial view.

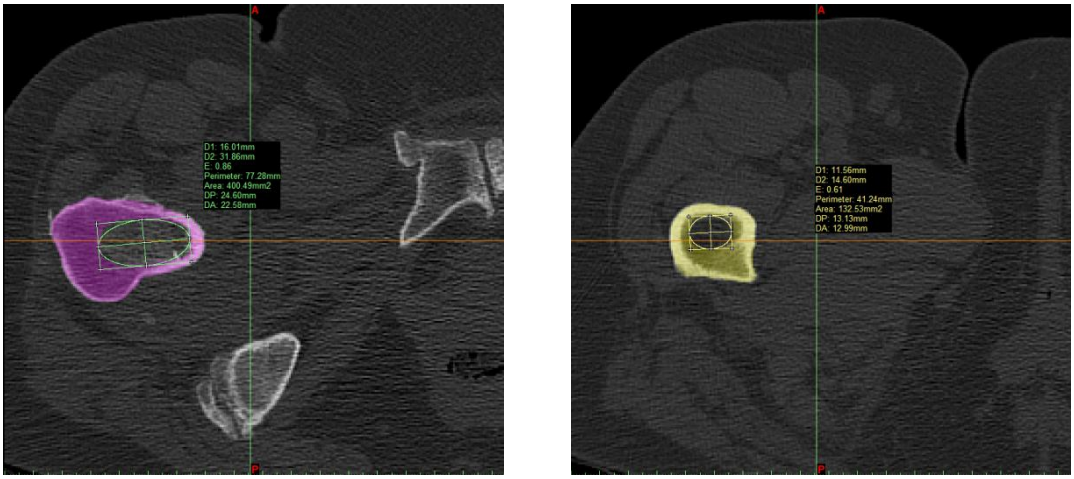

Figure 2.18 : Measurements to calculate per_m

a) Cavity's perimeter (proximal) ; b) Cavity's perimeter (distal)

Pressure p, calculated with [2.8] for each of the 5 patients, is summarized in Table 2.3:

Patient	Age	Gender	L_F [mm]	per_m [mm]	p [MPa]
1	50	M	59	64	5,5
2	42	M	54	61	6,3
3	60	F	60	69	5,0
4	59	F	60	69	5,0
5	19	M	56	56	6,7

Table 2.3 : Applied Pressure for FRI assessment

2.3.4. Fracture Risk Index Evaluation

Once the boundary conditions have been set, the FE mechanical simulation can be performed. To determine the FRI, the distribution of the maximum principal elastic strain (ε_{max}) is computed.

The average ε_{max} calculated for each FE of the model are compared to the critical value ε_{crit} = 7300 $\mu\varepsilon$, which represents the limit over which fracture occurs due to tensile strains, according to [68].

Thus, Fracture Risk Index, is defined by:

$$FRI\ [\%] = \frac{\varepsilon_{max}}{\varepsilon_{crit}} * 100 \qquad [2.9]$$

Fracture Risk is scoped into 7 specific zones of the proximal femur, manually selected from the surface. Each zone has a selected area of circa 200 mm^2, in which the average value of the maximum principal elastic strain is calculated to assess the FR. The zones are: 1) Greater Trochanter; 2) Calcar; 3) Anterior; 4) Posterior; 5) Inter-trochanteric Line; 6) Inter-trochanteric Crest; 7) Lesser Trochanter, according to [10].

Figure 2.19 : The 7 zones for FR, according to [10]
Greater Trochanter zone is evaluated in the lateral side of the bone.

2.4. Bone Mineral Density Changes

The evaluation of the Bone Mineral Density changes of the periprosthetic proximal femur is important to assess the behavior of the bone remodeling after the stem's implantation. BMD is assessed by comparing measures taken 24 hours and 12 months after the surgery.
To reach this goal, for each patient, Post 24h and Post 1y CTs are considered and processed in Mimics, after a proper conversion of the original DICOM dataset.

2.4.1. Reslicing

The two CT-Scans after THA are carried out in two different temporal circumstances.
Even if the CT scanner machine and its settings are the same, patient's body position can't be totally identical in the two acquisitions: sometimes, for instance, the same leg may be rotated with different angles, as it can be easily checked out in Figure 2.20.

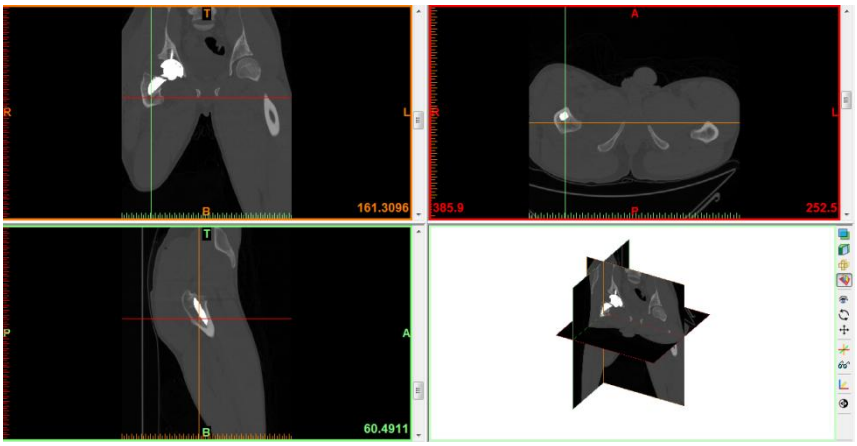

a)

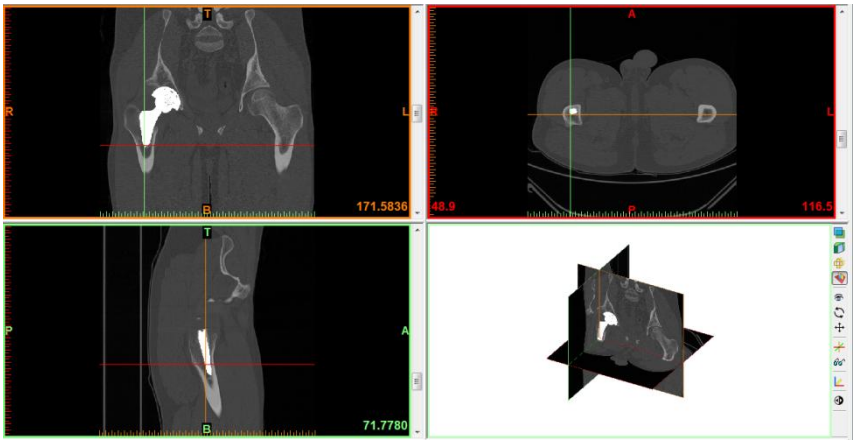

b)

Figure 2.20 : Different femur positions between Post 24h (a) and Post 1y (b).

Therefore, it can be very complicated to directly compare the two CT scans to evaluate BMD changes occurring in corresponding areas of the bone.

For this reason, it has been decided to use the Reslice Project Mimics tool with the principal aim of aligning the orientation of the body to ease the following images registration.

Moreover, with this tool, pixel size of the two images is uniformed, since it is possible to specify it before reslicing. Pixel size modification is applied to one of the two images, namely that with the highest value (lowest resolution). Its pixel value is modified setting it to other image's one, i.e. to the lowest value (highest resolution).

Furthermore, reslicing is also useful to crop the area of interest, i.e. the proximal femur, from the whole image for a clearer analysis.

Images can be resliced according to a straight line drawn in one of the three views.

Thus, both Post 24h and Post 1y are resliced following a common line, that has chosen to be the longitudinal axis of the stem, which can be selected in the coronal view.

Always to allow an easier comparison between Post 24h and Post 1y, reslicing line is traced starting from 2 cm below stem's tip, in order to have a common initial axial slice, that is to say a common reference for the resliced images. Reslicing line ends 2 cm above the proximal extremity.

An example of how the Reslicing Project tool works is shown in Figures 2.21 and 2.22 .

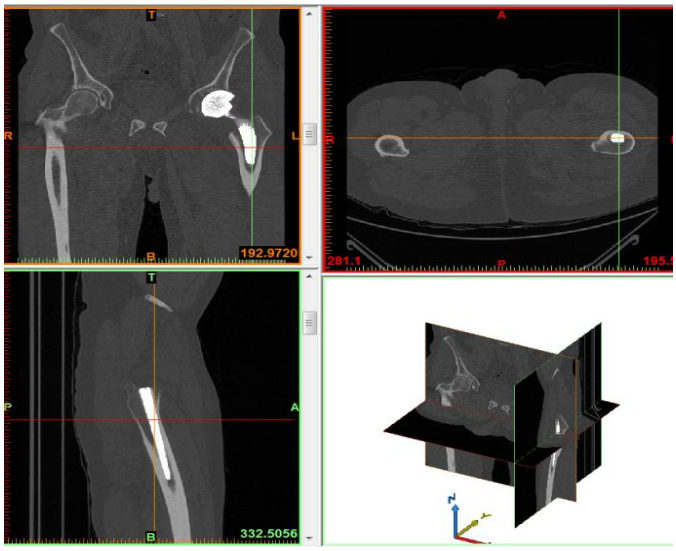

Figure 2.21 : Mimics project before Reslicing

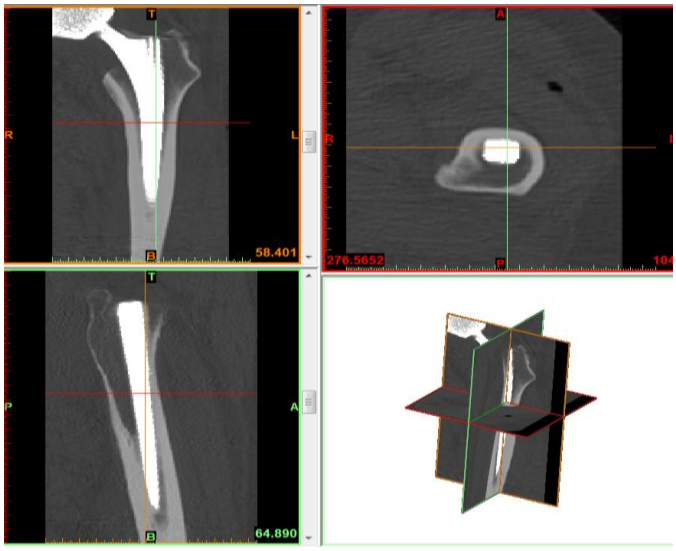

Figure 2.22 : Mimics project after Reslicing

2.4.2. Segmentation

In order to separate the interesting anatomical part from the rest of the body, a Segmentation operation is carried out through Mimics in both Post 24h and Post 1y images.
This means that pixels with a HU value belonging to a certain range are grouped together into a mask.

Since proximal femur is the interesting anatomical part, the thresholding range of values has been set to 255 HU - 3070 HU, where 255 HU is considered to be the lowest value for the cancellous bone, while 3070 HU is the highest value for the cortical bone, adapting from previous studies [54].

By using a similar procedure, a mask of the stem (unique threshold value: 3071 HU) is created. Later on, a Boolean operation is carried out to delete pixels belonging to the stem from bone mask (Minus operation).

Finally, additional manual fine tuning is done to get rid of artifacts, e.g. due to stem's metal. An example of the final femur bone mask can be seen in Figure 2.23.

By checking on Mask Properties tool, it is possible to get interesting information about the average HU of the mask.

According to the approach suggested in [79], average HU of 5 different axial slices (masks made of just a single slice) are recorded for both Post 24h and Post 1y femurs, for each patient.

Listed from the most proximal to the most distal, the 5 regions of interest are (Figure 2.24): 1) greater trochanter; 2) lesser trochanter; 3) 5 cm proximal to stem's tip; 4) stem's tip; 5) 2 cm distal to stem's tip.

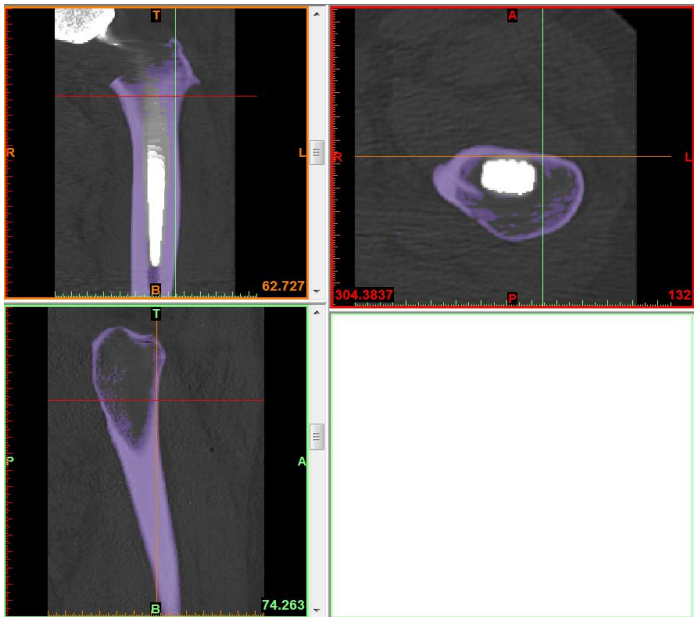

Figure 2.23: Femur bone mask (highlighted in purple)

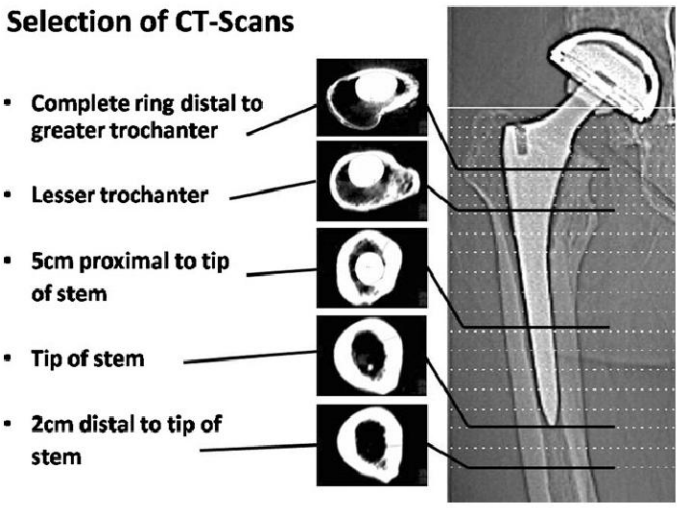

Figure 2.24: 5 Regions of Interest for BMD, from [79]

2.4.3. Image Registration and Subtraction

For a realistic evaluation of BMD changes over 1 year after THA, corresponding areas of the bone must be considered.

To make this happen, Post 24h and Post 1y images are registered together using Image Registration tool.

Mimics realizes a point-based registration by selecting 5 landmarks belonging either to the femur or to the stem, which are in common between the two images (Fig. 2.25).

The 6 reference points have been chosen with the criterion of being anatomical landmarks and being easily detectable in both images.

These landmarks are (Fig. 2.26):

1) stem's tip

2) protuberance under greater trochanter (distal end of the attachment site for gluteus minimus)

3) top of greater trochanter

4) lesser trochanter

5) gluteal tuberosity in axial view

6) protuberance of pectineal line in axial view.

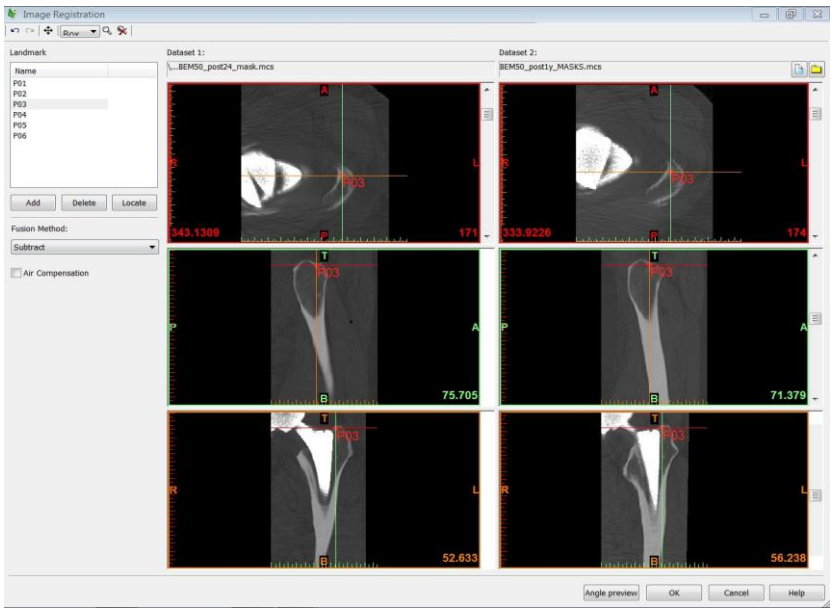

Figure 2.25 : Point-based Image Registration

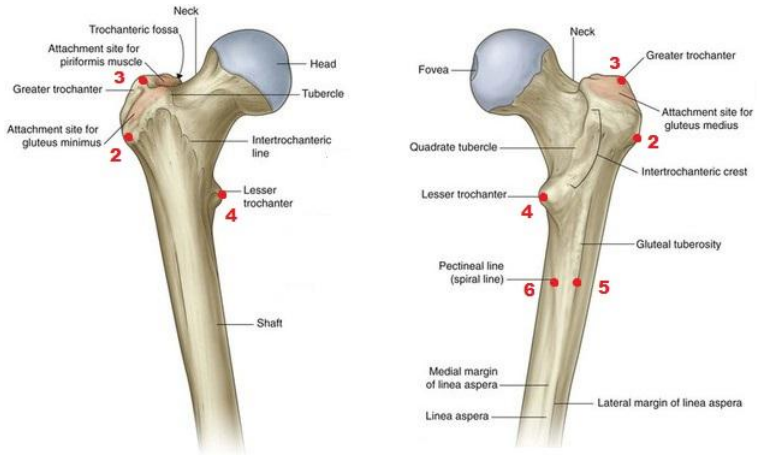

Figure 2.26 : Landmarks for Registration. Landmark 1 (stem's tip) not visible

Once the 6 landmarks have been placed, the Subtract Fusion Method is selected to carry the registration out.

With this type of Fusion Method a new Mimics project is created, having dataset of image 2 registered on dataset of image 1, and the part intersecting with dataset 1 fused with dataset 1 according to the following criterion:

$$GV_r = \begin{cases} GV_1 - GV_2, & GV_1 > GV_2 \\ 0, & GV_1 \leq GV_2 \end{cases}$$

Given GV_r as a generic voxel's GV in the newly created Mimics project.

Looking at the criterion, it results that registration operation needs to be repeated twice, since Mimics' Subtract Fusion Method sets to "black" ($GV_r = 0$) all the voxels with either negative or null GV_r, assigning a certain level of gray only if GV_r is positive.

Therefore, one registration + subtraction procedure is made to evaluate bone gain, while the other one is made for bone loss. For bone gain analysis, Post1y is selected to be the dataset 1, while Post 24h is the dataset 2; vice versa, for bone loss evaluation, Post 24h is set as dataset 1 and Post 1y as dataset 2. For more clearness, Table 2.4 summarizes these operations:

DATASET 1	FUSION METHOD	DATASET 2	RESULT
1 y	Subtract	24 h	**GAIN**
24 h	Subtract	1 y	**LOSS**

Table 2.4 : Subtraction Fusion Method

An example of the final result of images subtraction is given in Figure 2.27.
The “whiter” are the pixels, the higher is the difference in terms of BMD, that is to say, the more the bone has increased/decreased its quality.

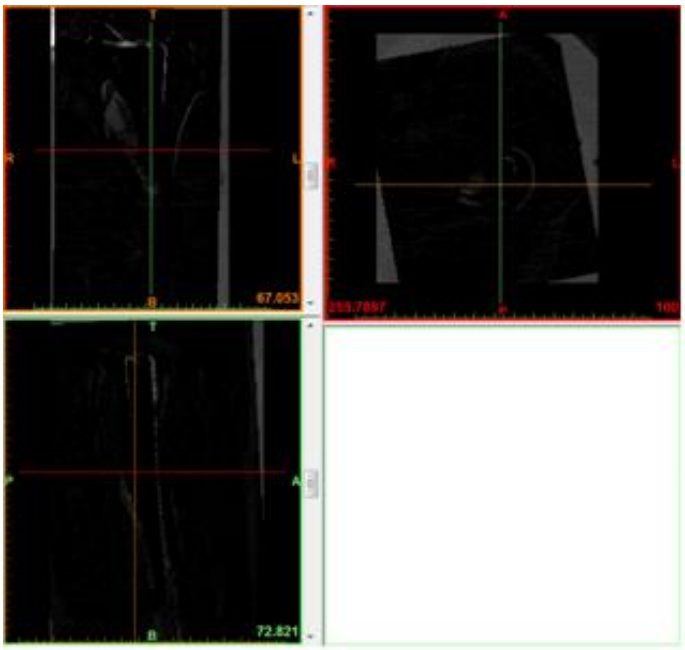

Figure 2.27 : Subtract Fusion Method (in this specific case, Post 24h - Post 1y)

2.4.4. Bone Mineral Density Gain and Loss Evaluation

Once the subtraction has been completed, a qualitative and quantitative analysis about BMD changes can be realized.

For clearness, in this paragraph, GVs will be defined as ΔGVs, since BMD changes analysis is carried out in the new Mimics Projects generated from Subtraction.
The below-described steps are separately applied to each new Mimics Project, therefore bone resorption and bone growth are independently evaluated.

First step is to import the masks of the Post 24h and Post 1y femurs (see § 2.4.2) in order to consider just the interesting pixels belonging to the bone.
Later on, a new mask is created with the Thresholding segmentation tool by selecting all the pixels whose ΔGrayValue is over 111. We will refer to this mask as the “Threshold Mask”.

Manipulating formula [2.1], and thinking in GV rather than HU (subtraction is done by Mimics operating on GVs), it is easy to get to the relationship [2.10]:

$$\Delta BMD \left[{}^{g}/_{cm^3}\right] = 0.000902\ \Delta GV \qquad [2.10]$$

Inserting ΔBMD = 0.1 g/cm^3 in [2.10], 111 ΔGV is obtained: this corresponds to the minimum significant value of BMD change, meaning that a BMD loss (or equivalently a BMD gain) lower than 0.1 g/cm^3 is not considered to be relevant.
This threshold value has been chosen considering inter-subject variability of QCT measurements of trochanteric cortical bone assessed in prior studies [59]. This value has been corrected with a coverage factor of 2, since data available in [59] allowed a more accurate evaluation.

Other source of error affecting a precise BMD changes evaluation is the misalignment between the two registered images, since the 6 landmarks are selected manually and femur masks (in Post 24h and Post 1y) cannot be totally superimposable. The result of the misalignment can be seen in Figure 1.10 in the brighter lines shaping just one side of femur's contour.
To overcome this issue, imported bone masks undergo a morphology operation of 3 pixels Erosion, that means circa 2 mm of the outer femur are not considered in the comparison between Post 24h and Post 1y bone mineral densities.

Successively, by doing a Boolean operation of Intersection between the Eroded Femur Mask and the Threshold Mask, the Final Mask is obtained. The latter is the target mask to look at for evaluating bone loss or gain.
As mentioned in § 2.4.3, the Post 1y-Subtract-Post 24h Mimics project is used to assess bone gain, while Post 24 h-Subtract-Post 1y is used to assess bone loss.
A scheme of the main steps is given in Figure 2.28:

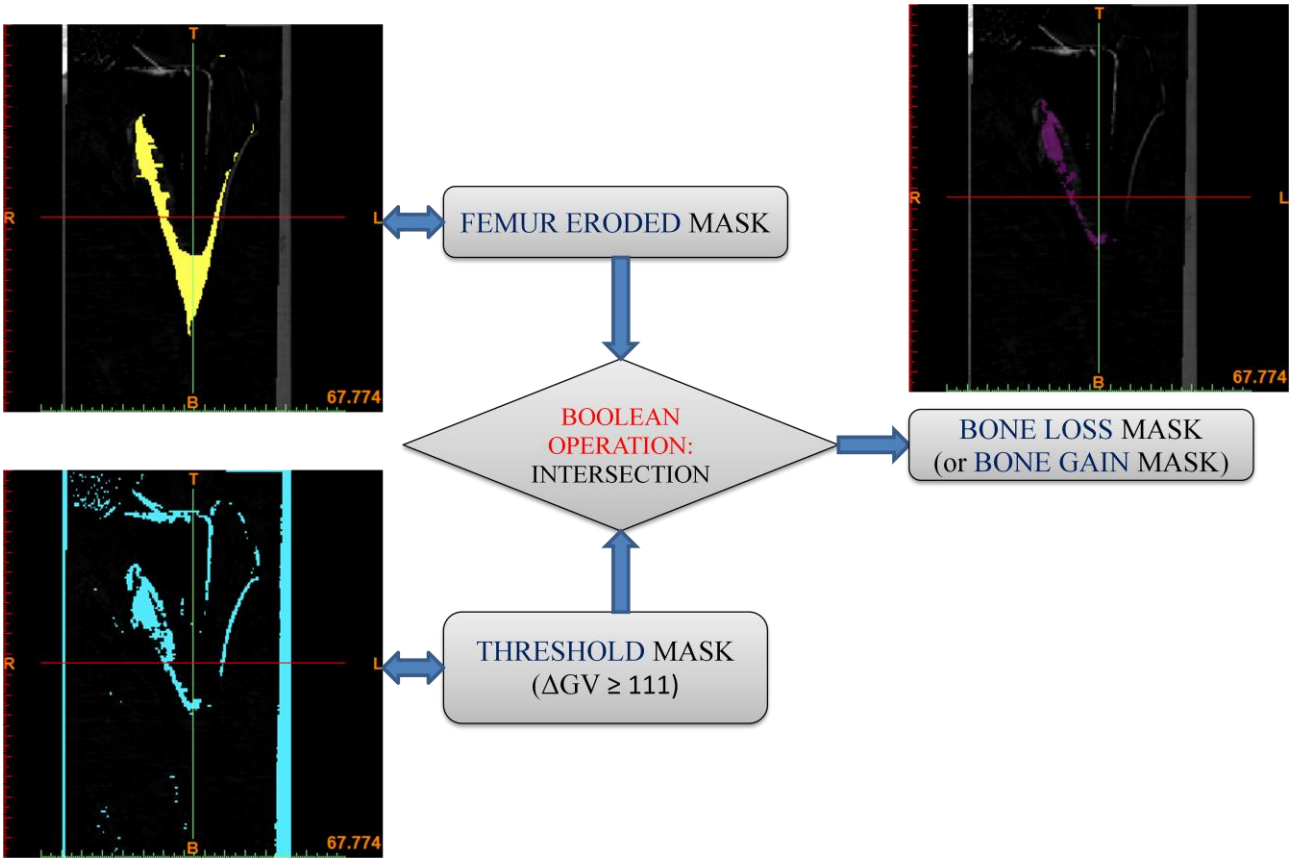

Figure 2.28 : Steps to evaluate bone loss/gain

Successively, by checking mask properties, information about the volume (in [mm^3]) of bone lost (or gained) is obtained, along with the HU distribution over femur mask.

Finally, a three-dimensional representation of the loss/gain areas over the proximal femur is realized, to better understand where the changes have occurred.

3. Results

3.1. Fracture Risk Index

Each of the 3D models consists of a finite elements number included between 258150 and 320371.
The FE analysis has been performed for all of 5 patients selected for this study.

The results of the FE simulation, in terms of maximum principal elastic strain distribution, can be visualized in Fig. 3.1. Blue areas represent “safe” zones, that is to say the calculated ε_{max} do not exceed the failure value ε_{crit} = 7300 $\mu\varepsilon$; otherwise, red colored parts of the bone reveal the zones where local fractures are very likely to occur. Moreover, the numerous presence of red/orange element inside the cavity of the femur is due to the fact that in these areas there are lots of “soft” elements, as already explained in § 2.3.3.1.

Fracture Risk Index has been calculated for 7 areas of investigation, in order to provide a quantitative method to assess which anatomical part of the proximal femur is more likely to fracture consequently to stem insertion.

Results show that Intertrochanteric Line and Intertrochanteric Crest areas are the most vulnerable areas, having respectively 82% and 66% of average FRI. It is also pointed out that Lesser Trochanter and Greater Trochanter regions are at the smallest risk of failure (average FRI 7% and 6%, respectively). Patient #3 presents a failure in 4 areas out of 7, namely the most proximal areas on the anterior and posterior sides. Failure is also recorded for Patient #4, in the I L zone. (Summary in Table 3.1)

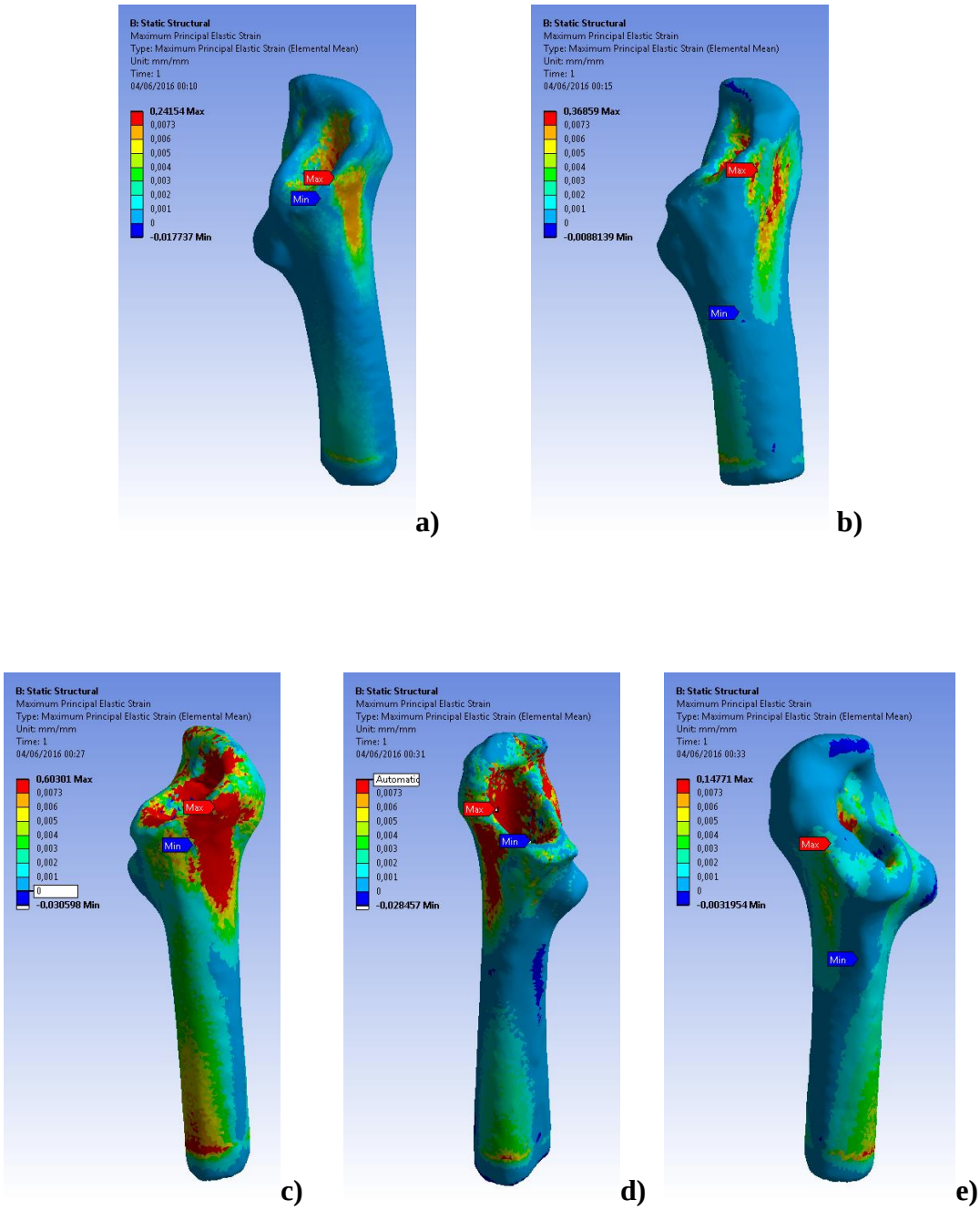

Figure 3.1: Results of FE analysis: Max Principal Elastic Strain Distribution

a) Patient 1, M 50; b) Patient 2, M 42; c) Patient 2, F 60; d) Patient 4, F 59; e) Patient 5, M 19

PATIENT	Age	G T	C	A	P	I L	I C	L T
1	50	4%	31%	67%	42%	69%	35%	2%
2	42	5%	28%	14%	23%	19%	33%	3%
3	60	14%	44%	Failure	Failure	Failure	Failure	22%
4	59	6%	39%	33%	84%	Failure	90%	7%
5	19	2%	20%	26%	13%	20%	33%	2%

Table 3.1: FRI in the 7 areas of investigation

Legend: G T = Greater Trochanter; C = Calcar; A = Anterior; P = Posterior; I L = Inter-trochanteric Line; I C = Inter-trochanteric Crest; L T = Lesser Trochanter.

The results of the FRI investigation is also plotted against age, showing that the highest risks of failure have been recorded for the eldest patients, aged 59 and 60. No failed regions have been found out for younger patients, namely 19, 42 and 50 years old ones. (Fig. 3.2):

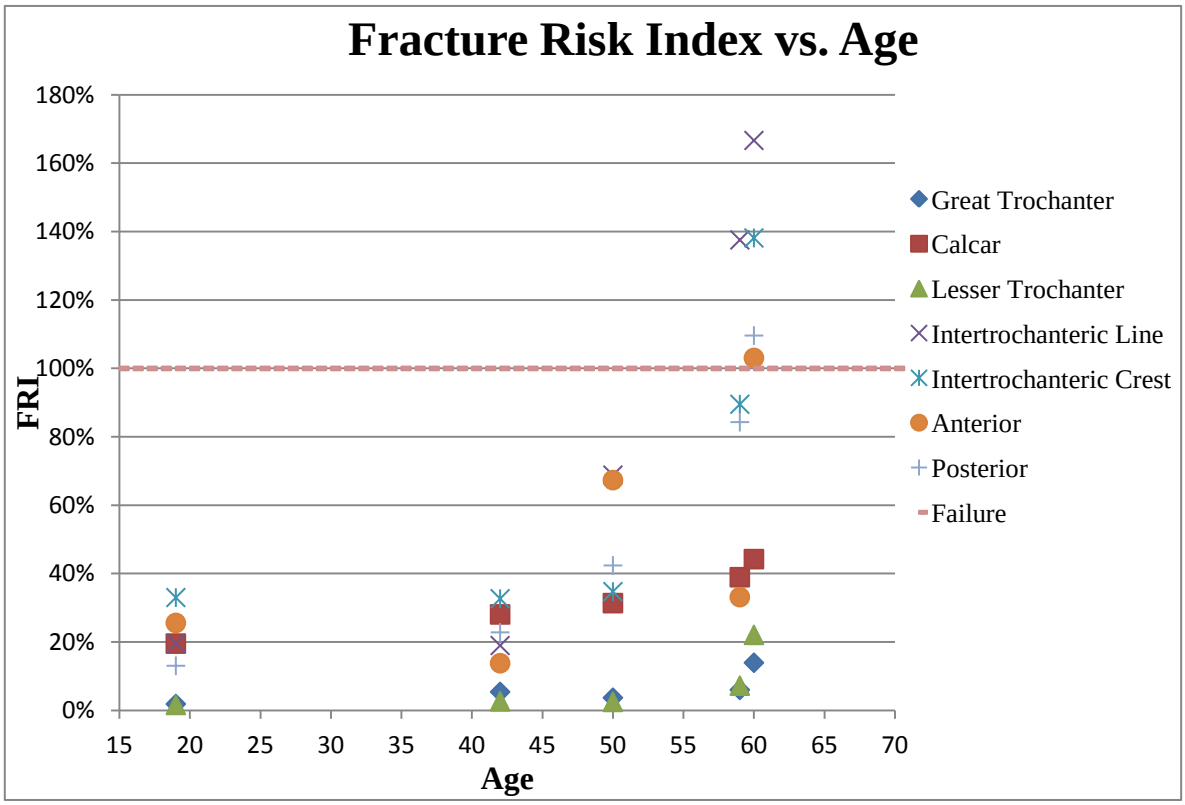

Figure 3.2 : Fracture Risk Indexes for different anatomical regions of the proximal femur plotted against patients' age

The percentage of elements having a maximum principal elastic strain over the critical threshold is also calculated. For this purpose, only elements with a ρ_{app} greater than 0.27 g/cm^3 (i.e. 255 HU) have been taken into account, namely just bony tissue (both cortical and cancellous) is considered for this specific evaluation. Patients #1, #2 and #5 show an overall percentage of fractured elements below 1%. For patients #3 and #4, instead, more than 2% of the total elements are expected to fail, respectively 5.48% and 2.68%.

Moreover, getting and processing data from Mimics, it is possible to examine the density distribution (calculated from HU) throughout the femur's 3D model of each patient. It is found out that ρ_{app} distribution profile is bimodal, like the one shown in Fig. 3.3; therefore, by means of a simple Matlab code, the two peaks of the distribution are measured. The peak corresponding to lower HU values is defined to be the average HU for cancellous bone, namely the average cancellous bone ρ_{app}. On the other hand, the peak measured for higher HU values corresponds to the average HU for cortical bone, that is to say its average ρ_{app}.

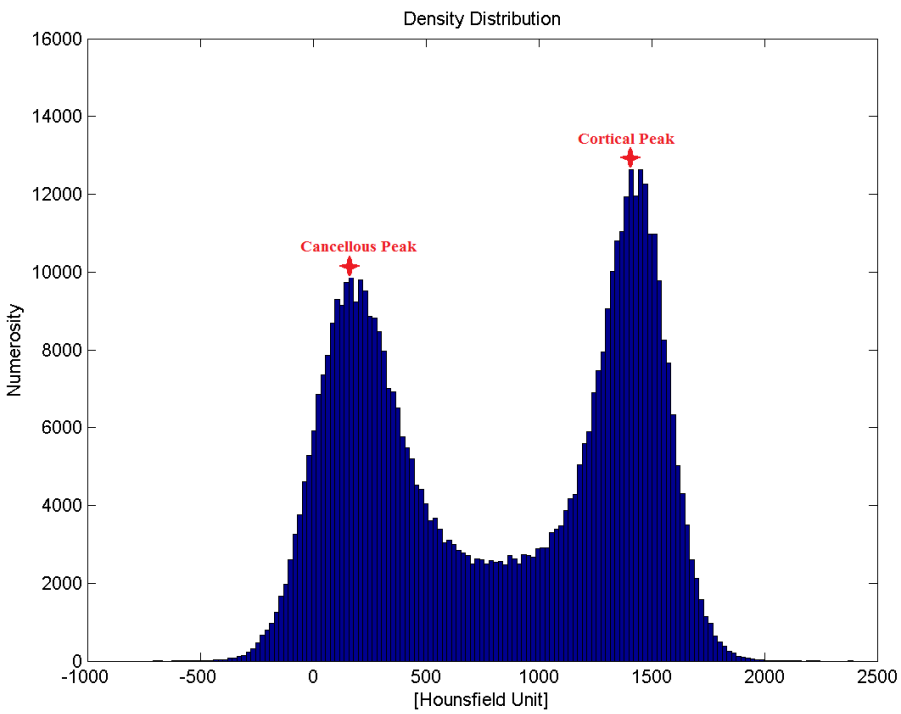

Figure 3.3 : HU distribution over the mask of the operated femur's 3D model. Cancellous and cortical peaks are indicated

Peaks calculated for each patient are compared to the number of fractured elements. (Fig. 3.4 and Fig. 3.5). Although it is hard to find a relevant relationship between average cortical density ($R^2 \approx 0.16$), a certain correlation is recognizable between spongy bone's average density ($R^2 = 0.76$), being aware that a more numerous sample would be required for a more significant statistical analysis.

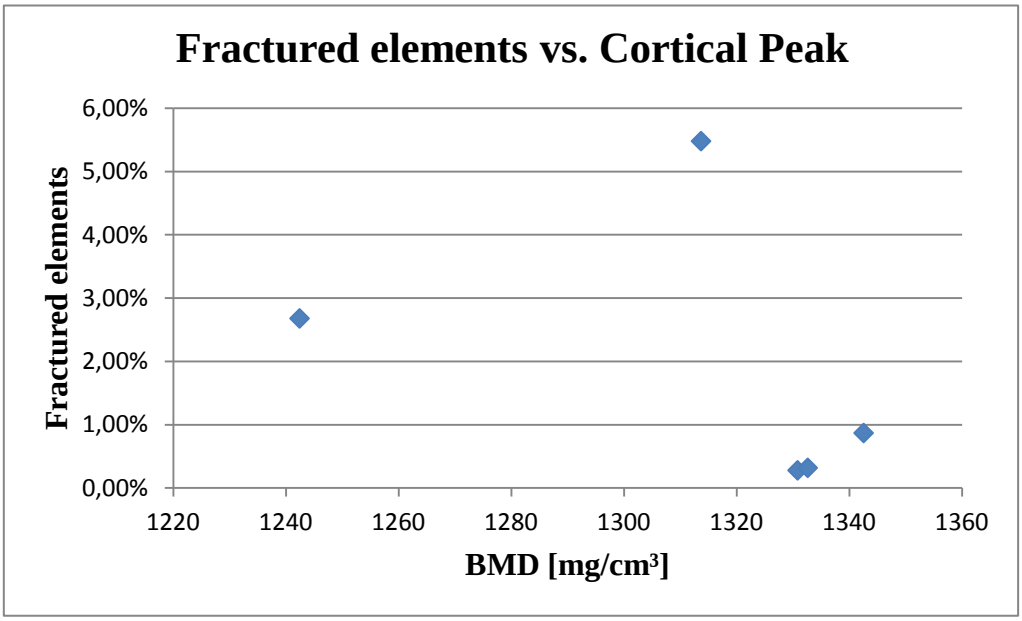

Figure 3.4 : Number of fractured elements against average density of cortical bone

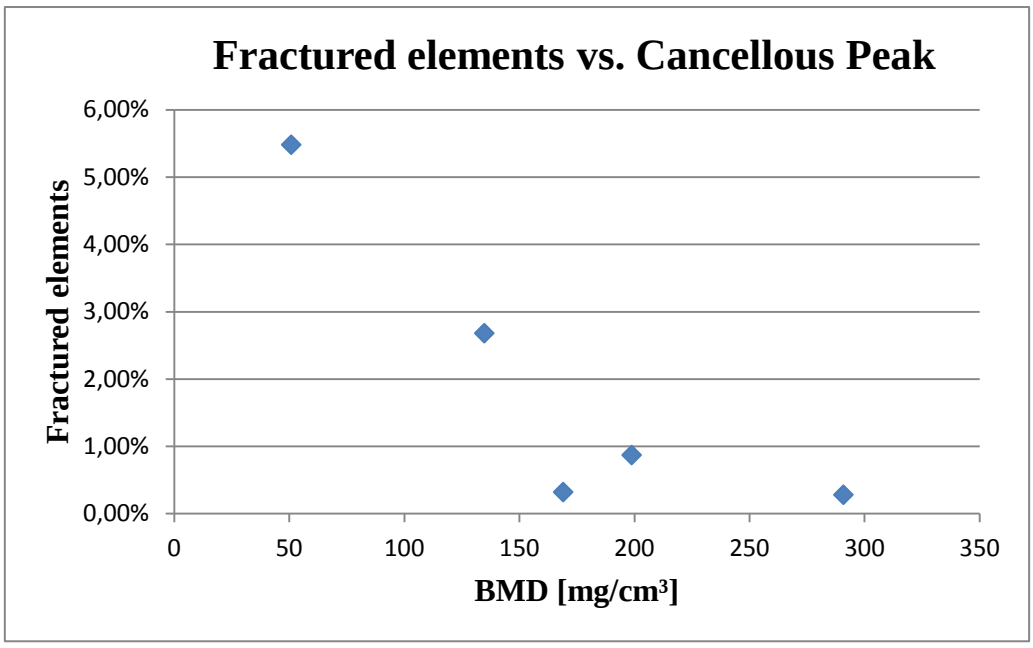

Figure 3.5 : Number of fractured elements against average density of trabecular bone

3.2. Bone Mineral Density Changes

Information taken from bone masks is used to assess BMD changes. Since in Mimics projects HUs (or ΔGVs) are assigned to pixels, formulas [2.1] and [2.10] are used to convert these values into volumetric BMD [g/cm^3].

For each patient, average BMD has been measured. Moreover, similarly to what has been done for FRI assessment, cortical bone peak has been registered as relevant information, too. Table 3.2 shows all the measured average BMD in [mg/cm^3], specifying how much Post 1y has changed compared to Post 24h.

Patient's no.	Post 24h	Post 1y	Difference
1	995	1004	+9
2	947	905	-41
3	991	935	-56
4	886	883	-4
5	862	874	+13

Table 3.2 : Average BMD [mg/cm3]

Table 3.3 reports the cortical bone peaks (in [mg/cm^3]) for all of the 5 patients:

Patient's no.	Post 24h	Post 1y	Difference
1	1324	1344	+21
2	1327	1314	-14
3	1312	1266	-46
4	1283	1250	-33
5	1351	1362	+11

Table 3.3 : Cortical BMD [mg/cm3]

3.2.1 BMD changes: 5 ROI

Results about BMD changes (in [mg/cm^3]) in the 5 ROI (see § 2.4.2) are now presented for all of the 5 subjects.

- **Patient #1, M, 50**

ROI	Post 24h	Post 1y	Difference
1	643	615	-4,4%
2	706	722	+2,3%
3	1049	1026	-2,2%
4	1064	1065	+0,1%
5	1071	1218	+13,7%

- **Patient #2, M, 42**

ROI	Post 24h	Post 1y	Difference
1	733	656	-10,5%
2	651	645	-0,8%
3	1021	1002	-1,9%
4	1030	1049	+1,8%
5	1053	1076	+2,1%

- **Patient #3, F, 60**

ROI	Post 24h	Post 1y	Difference
1	647	496	-23,4%
2	721	658	-8,8%
3	1047	959	-8,4%
4	1054	1013	-3,9%
5	1053	1010	-4,1%

- **Patient #4, F, 59**

ROI	Post 24h	Post 1y	Difference
1	513	466	-9,1%
2	633	577	-8,8%
3	923	866	-6,2%
4	950	977	+2,8%
5	945	968	+2,5%

- **Patient #5, M, 19**

ROI	Post 24h	Post 1y	Difference
1	728	458	-37,2%
2	786	537	-31,7%
3	1049	941	-10,3%
4	975	978	+0,3%
5	966	997	+3,3%

Figure 3.6 reports a summary of how much (in %) BMD has increased(+)/decreased(-) in one year after surgery. The percentage variations have been registered for each region of interest (ROI).

Average change in ROI 1 is -16.9(±13.3)%; in ROI 2 is -9.6(±13.3)%; in ROI 3 is -5.8(±3.7)%; in ROI 4 is +0.2(±2.6)%; in ROI 5 is +3.5(±6.4)%. The highest decrease has been registered in the greater trochanter region (ROI 1) for patient #5, while the highest BMD increase has occurred in ROI 5 (20 mm below stem's tip) for patient #1.

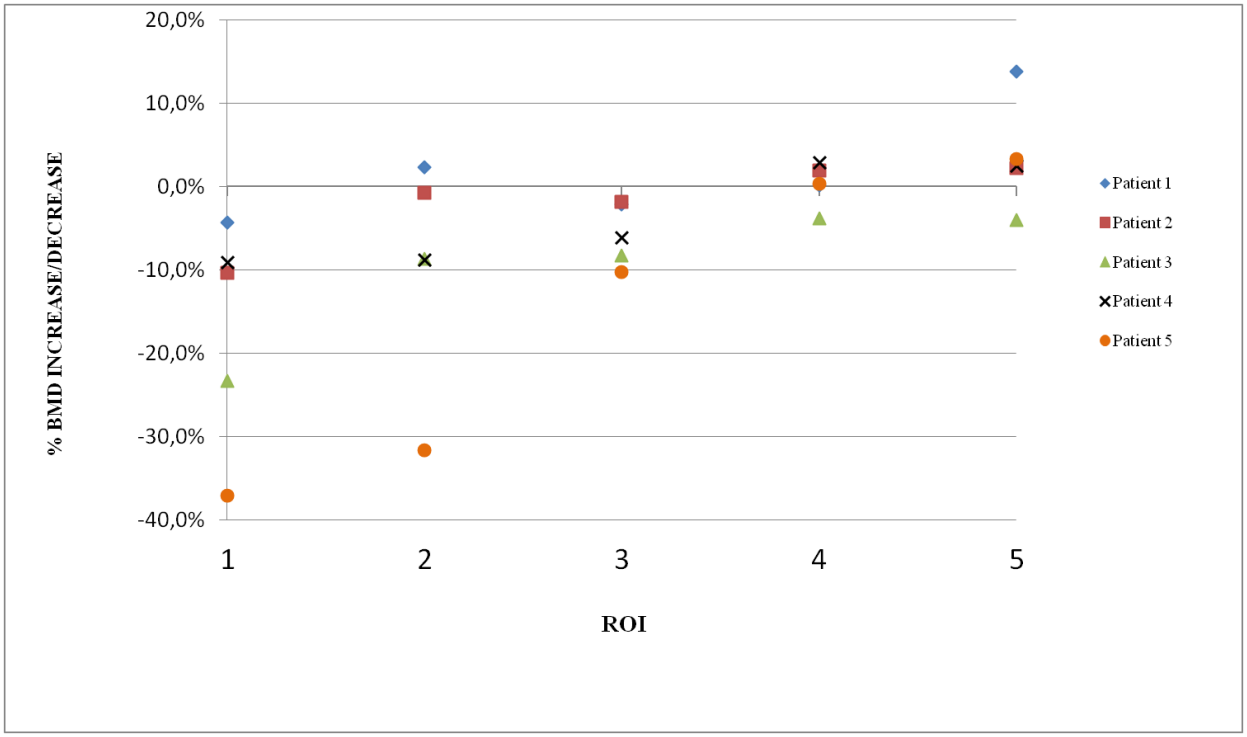

Figure 3.6 : % BMD changes in ROI

3.2.2 BMD changes: volume fractions

BMD loss and gain are calculated, in terms of volumes, as fractions of the entire femur's mask volume.

For clearness, it is fair to point out that here just the proximal part of the femur is considered, down to 20 mm distally to stem's tip.

The highest percentage of BMD decrease is recorded to be 11.7%, while the lowest is 4.4%.

With regard to BMD increase, the highest percentage registered is 4.0%, while the lowest one is 0.6%.

The average BMD lost volume fraction is 7.3±2.9 %, the average gained one is 1.7±1.4%.

Table 3.4 summarizes the calculated percentages of lost and gained volume.

Patient	Age	Gender	BMD Gain	BMD Loss
1	50	M	1.7%	4.4%
2	42	M	4.0%	8.3%
3	60	F	0.8%	5.6%
4	59	F	1.2%	6.3%
5	19	M	0.6%	11.7%

Table 3.4: BMD loss/gain volume fractions

These results have been compared to another approach to calculate BMD loss/gain developed at ETH Zurich [70].

Processing the same sample of 5 patients (identical input data) with this alternative protocol, the highest percentage of BMD decrease is 24.3%, while the lowest is 6.1%.

The highest increase is registered to be 8.5%, while the lowest is 0.2%.

The average BMD gained volume fraction is 3.4±3.2%, while the average lost volume fraction is 12.2±7.1%.

The results obtained with the alternative protocol are summarized in Table 3.5:

Patient	Age	Gender	BMD Gain	BMD Loss
1	50	M	1.2%	6.1%
2	42	M	8.5%	9.8%
3	60	F	3.1%	8.9%
4	59	F	4.1%	12.0%
5	19	M	0.2%	24.3%

Table 3.5 : BMD loss/gain volume fractions in ETH protocol

3.2.3. Comparison between two protocols

For each patient, a comparison between the method developed in this study and the ETH's protocol is carried out.

- **Patient #1: M, 50, L**

	New Protocol	ETH Protocol
BMD Loss	4,4%	6,1%
BMD Gain	1,7%	1,2%

3D distribution of Gain/Loss Areas:

Views	BMD GAIN	
	New Protocol	ETH Protocol
CORONAL PLANE – ANTERIOR		
CORONAL PLANE – POSTERIOR		
SAGITTAL PLANE – MEDIAL		
SAGITTAL PLANE - LATERAL		
3D		

Views	BMD LOSS	
	New Protocol	ETH Protocol
CORONAL PLANE – ANTERIOR		
CORONAL PLANE – POSTERIOR		
SAGITTAL PLANE – MEDIAL		
SAGITTAL PLANE - LATERAL		
3D		

- **Patient #2, M, 42, L**

	New Protocol	ETH Protocol
BMD Loss	8,3%	9,8%
BMD Gain	4,0%	8,5%

3D distribution of Gain/Loss Areas:

Views	**BMD GAIN**	
	New Protocol	**ETH Protocol**
CORONAL PLANE – ANTERIOR		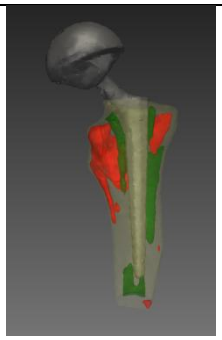
CORONAL PLANE – POSTERIOR		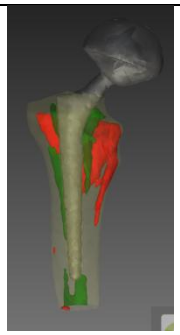

SAGITTAL PLANE – MEDIAL		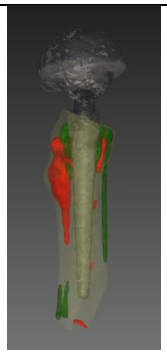
SAGITTAL PLANE - LATERAL		
3D		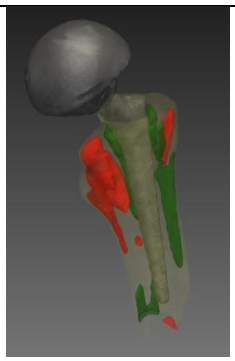

Views	BMD LOSS	
	New Protocol	ETH Protocol
CORONAL PLANE – ANTERIOR		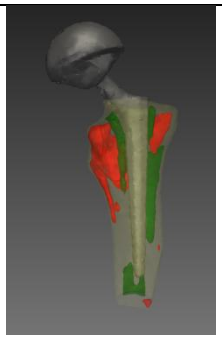
CORONAL PLANE – POSTERIOR		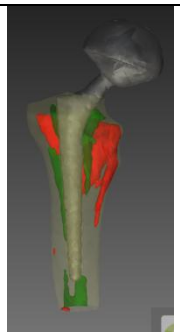
SAGITTAL PLANE – MEDIAL		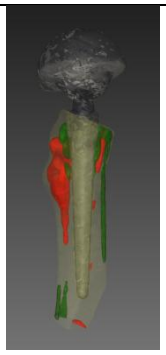
SAGITTAL PLANE - LATERAL		

3D		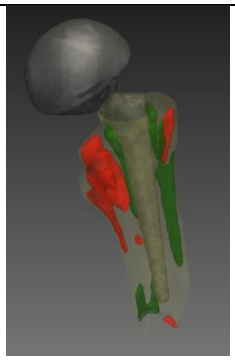

- **Patient #3, F, 60, L**

	New Protocol	ETH Protocol
BMD Loss	5,6%	8,9%
BMD Gain	0,8%	3,1%

3D distribution of Gain/Loss Areas:

Views	**BMD GAIN**	
	New Protocol	**ETH Protocol**
CORONAL PLANE – ANTERIOR		

CORONAL PLANE – POSTERIOR		
SAGITTAL PLANE – MEDIAL		
SAGITTAL PLANE - LATERAL		
3D		

Views	**BMD LOSS**	
	New Protocol	**ETH Protocol**
CORONAL PLANE – ANTERIOR		

CORONAL PLANE – POSTERIOR		
SAGITTAL PLANE – MEDIAL		
SAGITTAL PLANE - LATERAL		
3D		

- **Patient #4, F, 59, R**

	New Protocol	ETH Protocol
BMD Loss	6,3%	12,0%
BMD Gain	1,2%	4,1%

3D distribution of Gain/Loss Areas:

Views	**BMD GAIN**	
	New Protocol	**ETH Protocol**
CORONAL PLANE – ANTERIOR		
CORONAL PLANE – POSTERIOR		
SAGITTAL PLANE – MEDIAL		

SAGITTAL PLANE - LATERAL		
3D		

Views	**BMD LOSS**	
	New Protocol	**ETH Protocol**
CORONAL PLANE – ANTERIOR		
CORONAL PLANE – POSTERIOR		
SAGITTAL PLANE – MEDIAL		

SAGITTAL PLANE - LATERAL		
3D		

- **Patient #5, M, 19, R**

	New Protocol	ETH Protocol
BMD Loss	11,7%	24,3%
BMD Gain	0,6%	0,2%

3D distribution of Gain/Loss Areas:

Views	**BMD GAIN**	
	New Protocol	**ETH Protocol**

CORONAL PLANE – ANTERIOR		
CORONAL PLANE – POSTERIOR		
SAGITTAL PLANE – MEDIAL		
SAGITTAL PLANE - LATERAL		
3D		

Views	**BMD LOSS**	
	New Protocol	**ETH Protocol**

CORONAL PLANE – ANTERIOR		
CORONAL PLANE – POSTERIOR		
SAGITTAL PLANE – MEDIAL		
SAGITTAL PLANE - LATERAL		
3D		

4. Discussion

This work is part of the project born from the collaboration between Landspitali – University Hospital of Iceland and the Institute for Biomedical and Neural Engineering of Reykjavík University (RU), which aims to establish a clinical evaluation score for total hip replacement planning and for post-operative assessment, since currently orthopedic surgeons do not have any quantitative guideline for selecting the optimal implant, and they just rely on their experience and some qualitative evaluations for the choice.
The protocol of biomedical data collection includes that patients undergoing primary THR are CT-scanned three times: once before the operation and twice after it (24 hours and 1 year post-operatively).
CT-scans data is the source that provides information about volumetric BMD, which is the basic quantity for developing the assessment in silico methods here presented.

4.1. Fracture Risk

With regard to THR implant decision making support for clinicians, the aim of this work was to develop a novel method to simulate the mechanical response to the press-fitting of the cementless stem and to assess the intra-operative periprosthetic fracture risk for patients.
The assessment of FR was carried out by a finite element mechanical structural analysis of a 3D model of the femur, built with BMD information from pre-op CT scans.
The novelty of the method lies in the different approach towards FEM's boundary conditions, particularly about external loads. In fact, comparing to previous studies [53] [55], this method introduces a pressure-based load at the bone-stem interface, instead of a force-based one.
This allows to include relevant factors in the model, such as dimension of the bone (thus dimension of the implant), bone-metal frictional forces, stem's design and surgical hammer's force on the implant.
The results obtained from the FEA shows the feasibility and the repeatability of the method, since the same protocol can be applied for different patients respecting the automaticity and generality requirements of the subject-specific methods.
In particular, the FEA points out the possibility to get a map of the maximum principal elastic strain distribution over the periprosthetic bone, which allows to locate where the fracture is more likely to occur.

The analyses carried out on the 5 patients show that ROI subject to greater fracture risk are mainly the Intertrochanteric Line and in the Intertrochanteric Crest.
Patient #3 presented failure in 4 ROI out of 7, this suggests that maybe there is an overestimation of the loads involved.
There are some divergences with results of other protocols developed at the RU [55] [80], since Calcar zone is the most-critical area in these model. Differences could be expected beforehand, as load boundary conditions (2 equals and opposite forces, instead of a distributed pressure) and failure mechanical criteria (Von Mises equivalent stress instead of maximum principal strain) are different.
It is clear the needing of a validation: the reliability of one or another FE model must be checked with experimental evidences, for example post 24h DEXAs or CT-scans (which are better to locate fractures three-dimensionally) exhibiting a intra-operative fracture. (Fig. 4.1)
Moreover, a sensitivity analysis on how parameters identification errors propagate and affect the model's accuracy is needed to be done.
This study also outlines the possibility to investigate correlations between number of fractured elements – which is influenced by density of the mesh – and indicators for implant decision making, such as age, gender and above all bone quality.
Well-knowing that a larger cohort of patients is needed for a significant statistical support, data collected for 5 patients suggest that age is not the unique parameter to be considered while choosing the optimal implant: in fact bone mineral density, especially cancellous bone's one, may be a crucial factor influencing the risk of intra-operative fracture.
It is worth to repeat that a larger number of patients must be processed to statistically confirm these suppositions.

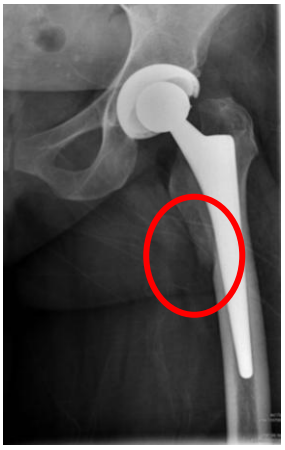

Figure 4.1 : Radiography taken a few days after cementless THR, demonstrating a possible intra-operative fracture. Courtesy of Landspitali – University Hospital of Iceland

Limits

The FE model is inevitably affected by errors. Firstly, CT-scans have a finite spatial resolution: one negative consequence of this feature is the partial volume effect, which can lead to the underestimation of the density of the outer bone tissue surface, and consequently, of its stiffness and its mechanical strength.
Also manual segmentation performed within the protocol introduces errors that imply an alteration of the surface geometry. This may lead to ignore relatively high density bone portions, which means to generate a mechanically less-resistant femur's model.
Accuracy of the model can be jeopardized by some aspects of the material assignment procedure.
Firstly, densitometry calibration laws are affected by errors linked to the measurements of the parameters that define the relationship; secondly, density-Young's modulus law does not consider distinction between cortical and cancellous bone.
Furthermore, bone is modelized and discretized with a finite number of elements; each of them is considered to be made of a single linear-elastic isotropic material: this is clearly a simplification of the complexity of bone's material and structural inhomogeneity.
Moreover, due to computational time constraints, the variety of materials has been limited to 50.
Finally, the FE model unveils limits for the assignment of boundary conditions. In fact, to define boundary conditions, groups of finite elements are manually selected, introducing inter-patients errors. Moreover, each parameter influencing the pressure's magnitude needs to be carefully defined for each of the subjects, and sometimes factors like bone-stem friction coefficient can be hard to define.

4.2. Bone Mineral Density Changes

CT-based densitometry measurements from post 24h and post 1y datasets are employed for developing an in silico method to assess proximal femur's BMD evolution 1 year after cementless THR.

The purpose of this study was to create a repeatable protocol to evaluate the three-dimensional changes of volumetric BMD around the cementless stem, giving qualitative and

quantitative hints on how much bone's volume has increased/decreased 1 year post-operatively.

It has been verified that the protocol is easily applicable to all the patients that underwent cementless THR, and no discouragements are seen that could prevent from use a similar method to assess BMD changes for cemented THR, too.

Using Mimics to process and compare post 24h and post 1y CT-scans allows to check the BMD differences in multiple ways.

Firstly, the average BMD can be measured from bone's mask information. Results show that differences between subjects can be vast.

As proposed in a study by Pitto et al. [79], in order to minimize reproducibility errors, BMD is measured in 5 ROI, that are easily recognizable in all the patients. Results suggest that the greatest BMD gain is registered 2 cm distally to the stem, while the greatest BMD loss is registered in the Greater Trochanter region which is substantially consistent with literature [79] [81].

Furthermore, the protocol introduces a way to assess three-dimensional distribution of BMD change. This assessment is performed both qualitatively and quantitatively. Indeed, it was possible to visualize a 3D model of the femur, in which significant volumetric BMD changes (both decrease and increase) are highlighted. A measurement of the lost/gained volume fraction, compared to the proximal bone's mask volume, is provided, too.

Outcomes of this protocol are compared to ETH's one [70]. ETH method's main difference is that the segmentation, the registration and the 3D model generation are automatically performed with an algorithm that utilizes different open-source softwares for the different steps of the protocol. In the method presented here, all the operation are carried out in Mimics environment and some of the operations are performed manually. This means that ETH process is quicker, but allows lesser control in process like segmentation and 3D model generation: therefore a higher loss of relevant information and a lesser detail in visualizing subject-specific results. Moreover, ETH protocol does not include BMD analysis for the 5 ROI.

However, at least qualitatively, three-dimensional BMD change assessments are similar for the two protocols, since zones of bone density loss and gain are located in analogous areas. On the other side, quantitative assessments of lost/gained volume fractions are numerically different, in fact the lost volume percentages are greater in ETH protocol for all of the 5 patients.

By analyzing the 3D results, it can be spotted that a considerable part of the lost volume in the ETH method is located in the outer surface of the bone. This can be an overestimation of BMD loss, since BMD changes in the outer surface may be due to misalignment during registration, and the protocol does not consider a solution to it.

Limits

There are some limitations that can affect the accuracy of BMD changes assessment.
First of all, by reason of standardization necessities of the protocol, bone's segmentation is performed by setting a lower and a upper HU thresholds, in order to pick only bone tissue. This thresholding operation inevitably leads to discard pixels that actually correspond to bone tissue, in particular the lower limit seems to be critical, since some of the patients may have cancellous bone with even lower HU. By the way, reducing the lower HU threshold leads to consider also soft tissue, that are undesirable for the purpose of this analysis.
Images registration process is a source of errors, too. In fact, manually setting the anatomical landmarks for the point-based rigid registration can affect the repeatability of the process, since inter-operator and intra-operator errors can be observed.
Moreover, the registration+subtraction operation between post 24h and post 1y images must be performed twice (one for gain and one for loss assessments) since Mimics does not allow to consider negative GVs as result of the subtraction, and this doubles the aforecited errors due to registration.
The choice of the threshold to evaluate significant variation of BMD is a critical issue as well, and a deeper analysis of the minimum ΔGV value will be requested in the future.
Misalignment of the registered images can also introduce errors in comparing BMD of homologous parts of the femur. As already explained in §2.4.4, a solution to solve this problem is not to consider the outermost volume of the femur by eroding the volume femur's mask. Indeed, an excessive number of eroded pixels leads to lose important information, while a too low number of eroded pixels implies an overestimation of the lost/gained volumetric BMD.

5. Future work and Conclusions

5.1. Fracture Risk

The method presented here must be validated and supported by a sensitivity analysis, as already mentioned. It can be further developed by adopting a different material mapping method, since it influences the accuracy of CT-based FE models. [82] For instance, it can be used the method indicated by Helgason et al. [83], in which material properties are allowed to vary spatially within each elements volume, that has been demonstrated to improve strains prediction accuracy.
Moreover, an additional improvement of the method would be to examine time-dependent loads, since a steady-state is here considered in the FE simulation.

The feasibility and repeatability of this method suggest that a larger cohort of patients (already enrolled in the main project and undergone cemented THR, as well) can be processed to find correlations between fracture risk and indicators like age, gender, cortical bone average density and cancellous bone average density. A statistical analysis of these data will be used to develop a database that will define a clinical score for future patients deciding to replace their hip. This will be a quantitative guideline for the implant decision making that will lead to the optimization of the preoperative planning, which can be eventually favorable to prevent from critical and expensive revision surgeries.

5.2. Bone Mineral Density Changes

Future work will include finding solutions to the mentioned limitations, such as better image registration and subtraction operations, in order to improve repeatability of the method and limiting operator-depending errors.
Once dealt with these problems, the presented method can be applied for the assessments of a larger cohort of patients, also with cemented prostheses.

With a statistical support, results of BMD changes 1 year after surgery can be correlated to factors like age, gender, prosthesis design or prosthesis material, aiming to assess the bone response to specific implants. This will serve for a validation of the model by comparing the results with established methods, like DEXA-based ones.
Moreover, BMD changes assessed with this method will be used to validate the 3D results of FE models [5] [65] [84] [85] for predictions of bone remodeling.

To conclude, it has been shown the feasibility of assessing three-dimensional BMD changes after THR surgery. Potentially, this method can have a clinical impact, since it can be a useful tool for many aspects. One of them is to validate predictive FE models of bone remodeling which can be used in future by clinicians to choose the proper THR implant.
Another aspect is to provide clinicians with a tool to monitor bone-prosthesis integration during post-operative follow-up.

References

[1] A. Abdulkarim, P. Ellanti and al., “Cemented versus uncemented fixation in total hip replacement: a systematic review and meta-analysis of randomized controlled trials,” *Orthop Rev*, no. 5, 2013.

[2] N. Hailer, G. Garellick and J. Kärrholm, “Uncemented and cemented primary total hip arthroplasty in the Swedish Hip Arthroplasty Register,” *Acta Orthop.*, no. 81, pp. 34-41, 2010.

[3] S. Morshed, B. KJ et al., «Comparison of cemented and uncemented fixation in total hip replacement: a meta-analysis.,» *Acta Orthop.*, vol. 3, n. 78, pp. 315-326, 2007.

[4] M. Wyatt, G. Hooper et al., «Survival outcomes of cemented compared to uncemented stems in primary total hip replacement,» *World J Orthop.*, vol. 5, n. 5, pp. 591-596, 2014.

[5] R. Huiskes, H. Weinans et al., «The Relationship Between Stress Shielding and Bone Resorption Around Total Hip Stems and the Effects of Flexible Materials.,» in *SYMPOSIUM: 1991 PROCEEDINGS OF THE HIP SOCIETY*, 1992.

[6] D. R. Sumner and J. O. Galante, «Determinants of stress shielding: design versus interface,» *Clinical orthopaedics and related research*, vol. 274, pp. 202-212, 1992.

[7] J. McLaughlin, «Total Hip Arthroplasty with an Uncemented Tapered Femoral Component,» *The Journal of Bone and Joint Surgery (American)*, vol. 90, n. 6, pp. 1290-1296, 2008.

[8] D. Taaffe, J. Cauley, M. Danielson et al., «Race and sex effects on the association between muscle strength, soft tissue, and bone mineral density in healthy elders: the Health, Aging and Boddy Composition Study,» *Journal of Bone and Mineral Research*, vol. 16, n. 7, pp. 1343-1352, 2001.

[9] P. Gargiulo and H. Jónsson Jr, «Clinical evaluation score for Total Hip Arthroplasty

planning and post-operative assessment,» Reykjavik, 2014.

[10] Þ. Pétursson, Bone Mineral Density and Fracture Risk Assessment for Patients Undergoing Total Hip Replacement, Reykjavik (Iceland): Reykjavik University, 2013.

[11] J. Bilezikian, L. Raisz and T. Martin, Principles of Bone Biology, Academic Press, 2008.

[12] S. C. Cowin, *Bone Mechanincs Handbook,* CRC Press, 2001.

[13] N. M. B. Willems, G. E. J. Langenbach, V. Everts and A. Zentner, «The microstructural and biomechanical development of the condylar bone: a review,» *The European Journal of Orthodontics,* pp. 479-485, 2013.

[14] *Copyright 2006 Pearson Education, Inc. publishing as Benjamin Cummings.*

[15] S. Cowin, W. V. Buskirk and R. Ashman, “Properties of bone,” in *Handbook of Bioengineering,* New York, McGraw Hill, 1987, p. Chapt. 2.

[16] L. J. Raggatt and N. C. Partridge, "Cellular and Molecular Mechanisms of Bone Remodeling," *The Journal of Biological Chemistry,* no. 285, pp. 25103-25108, 2010.

[17] D. Carter, “Mechanical loading histories and cortical bone remodeling,” *Calcified Tissue International,* vol. 36, pp. S19-S24, 1984.

[18] L. Lanyon and C. Rubin, «Static vs dynamic loads as an influence on bone remodelling,» *Journal of Biomechanics,* vol. 17, pp. 897-905, 1984.

[19] L. Cristofolini, «In vitro evidence of the structural optimization of the human skeletal bones,» *Journal of Biomechanics,* vol. 48, pp. 787-796, 2015.

[20] P. M. Cawthon, “Gender Differences in Osteoporosis and Fractures,” *Clinical Orthopaedics and Related Research,* vol. 469, no. 7, pp. 1900-1905, 2011.

[21] A. Parfitt, «Age-related structural changes in trabecular and cortical bone: Cellular mechanisms and biomechanical consequences,» *Calcified Tissue International,* vol. 36, pp. S123-S128, 1984.

[22] X. Wang, X. Shen, X. Li and C. Agrawal, «Age-related changes in the collagen network and toughness of bone.,» *Bone,* vol. 31, n. 1, pp. 1-7, 2002.

[23] R. Huiskes, «Stress Shielding and Bone Resoption in THA: Clinical versus Computer-Simulation Studies,» *Acta Orthopoedica Belgica,* vol. 59, pp. 118-129, 1993.

[24] L. Cristofolini, «A Critical Analysis of Stress Shielding Evaluation of Hip Prostheses,» *Critical Reviews™ in Biomedical Engineering,* vol. 25, pp. 409-483, 1997.

[25] "Teach Me Anatomy.info," [Online]. Available: http://teachmeanatomy.info/lower-limb/joints/the-hip-joint/.

[26] A. Biel, Trail Guide to Movement: Building the Body in Motion, Books of Discovery, 2014.

[27] S. Pramanik, A. Agarwal and K. Rai, "Chronology of Total Hip Joint Replacement and Materials Development," *Trends Biomater. Artif. Organs,* vol. 19, no. 1, pp. 15-26, 2005.

[28] R. Crawford and D. Murray, «Total hip replacement: indications for surgery and risk factors for failure,» *Ann Rheum Dis,* vol. 56, pp. 455-457, 1997.

[29] R.I.P.O., «HIP, KNEE AND SHOULDER ARTHROPLASTY IN EMILIA ROMAGNA (ITALY),» Servizio Sanitario Regionale Emilia-Romagna, 2015.

[30] C. Engh and W. Culpepper, «Long-term results of use of the anatomic medullary locking prosthesis in total hip arthroplasty.,» *J Bone Joint Surg Am,* vol. 79, n. 2, pp. 177-184, 1997.

[31] S. Birtwistle, K. Wilson and M. Porter, "Long-term survival analysis of total hip replacement," *Ann R Coll Surg Engl.,* vol. 78, no. 3, pp. 180-183, 1996.

[32] OECD, «HEALTH AT A GLANCE 2015,» 2015.

[33] "Database Schede di Dimissione Ospedaliera," 2001-2012.

[34] “Mr Evert Smith MBBCh BSc FRCS,” [Online]. Available: http://evertsmith.com/innovations/.

[35] U. Holzwarth and G. Cotogno, «Total Hip Arthroplasty,» JRC Scientific and Policy Reports, European Commission, 2012.

[36] R. Brand, J. Callaghan and R. Johnston, “Total hip reconstruction,” *Iowa Orthop J,* vol. 11, pp. 19-42, 1991.

[37] M. Joshi, S. Advani et al., “Analysis of a femoral hip prosthesis designed to reduce stress shielding,” *J Biomech,* vol. 33, no. 12, pp. 1655-1662, 2000.

[38] G. Demey, C. Fary and S. Lustig, “Does a collar improve the immediate stability of uncemented femoral hip stems in total hip arthroplasty? A bilateral comparative cadaver study,” *J Arhtroplasty,* vol. 26, pp. 1549-1555, 2011.

[39] T. Wik, «Experimental evaluation of new concepts in hip arthroplasty,» *Acta Orthop,* vol. 83, pp. 1-26, 2012.

[40] S. Smith, D. Dowson and A. Goldsmith, «The effect of femoral head diameter upon lubrication and wear of metal-on-metal total hip replacements,» *Prost Inst Mech Eng,* vol. 215, pp. 161-170, 2001.

[41] D. W. Manning, P. Chiang, J. Martell, J. Galante and W. Harris, “In vivo comparative wear study of traditional and highly crosslinked polyethylene in total hip arthroplasty,” *J Arhtroplasty,* vol. 20, pp. 880-886, 2005.

[42] I. D. Learmonth, C. Young and C. Rorabeck, “The operation of the century: total hip replacement,,” *Lancet,* vol. 370, pp. 1508-1519, 2007.

[43] S. J. Charnley, “The bonding of prostheses to bone by cement,” *J Bone Joint Surg Br,* Vols. 46-B, pp. 518-529, 1964.

[44] L. A. Müller, N. Wenger, M. Schramm, D. Hohmann, R. Forst and H. Carl, “Seventeen-year survival of the cementless CLS Spotorno Stem,” *Archives of Orthopaedic and*

Trauma Surgery, vol. 130, no. 2, pp. 269-275, 2009.

[45] J. R. McLaughlin, «Total Hip Arthroplasty with an Uncemented Tapered Femoral Component,» *The Journal of Bone and Joint Surgery (American),* vol. 90, n. 6, 2008.

[46] Z. Inc., «CLS® Spotorno® Hip Stem - Surgical Technique,» [Online]. Available: www.zimmer.com/.

[47] J. J. Callaghan, A. G. Rosenberg and H. E. Rubash, "PressFit Femoral Components," in *The Adult Hip,* Lippincott Williams & Wilkins, 1998, pp. 1085-1092.

[48] C. Schmidler, «HealthPages.org,» 2015. [Online]. Available: http://www.healthpages.org/surgical-care/hip-joint-replacement-surgery/.

[49] D. D. D'Lima, C. S. Oishi, W. J. Petersilge, C. W. C. Jr and R. H. Walker, "100 cemented versus 100 noncemented stems with comparison of 25 matched pairs," *Clin. Orthop. Relat. Res,* vol. 348, pp. 140-148, 1998.

[50] G. Ni, W. Lu, K. Chiu and F. DY, «Cemented or uncemented femoral component in primary total hip replacement? A review from a clinical and radiological perspective.,» *J Orthop Surg (Hong Kong),* vol. 13, n. 1, pp. 96-105, 2005.

[51] C. A. Engh, A. H. Glassman and W. L. Griffin, «Results of cementless revision for failed cemented total hip arthroplasty,» *The Journal of Bone & Joint Surgery - British Volume,* vol. 235, pp. 91-110, 1988.

[52] G. Hooper, M. Stringer and A. Rothwell, «Early revision for cemented & cement-less primary total hip arthroplasty: an analysis of the New Zealand Joint Registry,» *Journal of Bone & Joint Surgery, British Volume,* Vol. %1 di %291-B, pp. 336-337, 2009.

[53] T. Pétursson, K. Edmunds, M. Gislason, B. Magnusson, P. Gargiulo et al., «Bone Mineral Density and Fracture Risk Assessment to optimize Prosthesis Selection in Total Hip Replacement,» *Computational and Mathematical Methods in Medicine,* 2015.

[54] P. Gargiulo, T. Helgason, P. Reynisson et al., «Monitoring of Muscle and Bone Recovery in Spinal Cord Injury Patients Treated With Electrical Stimulation Using

Three-Dimensional Imaging and Segmentation Techniques: Methodological Assessment,» *Artificial Organs,* vol. 35, pp. 275-281, 2011.

[55] P. Gargiulo, B. magnusson, B. Helgason et al., «Bone Mineral Density and Fracture Risk assessment for patients undergoing total hip arhtroplasty as support for decision making,» *European International Journal of Science and Technology,* vol. 2, n. 5, pp. 96-104, 2013.

[56] J. J. Schreiber, P. A. Anderson, H. G. Rosas, A. L. Buchholz and A. G. Au, «Hounsfield units for assessing bone mineral density and strength: a tool for osteoporosis management,» *The Journal of Bone & Joint Surgery,* vol. 93, pp. 1057-1063, 2011.

[57] L. Goldman, «Principles of CT and CT Technology,» *Journal of Nuclear Medicine Technology,* vol. 35, pp. 115-128, 2007.

[58] R. Ciernak, X-ray Computed Tomography in Biomedical Engineering, London: Springer-Verlag, 2011.

[59] X. Cheng, G. Lowet, S. Boonen et al., «Assessment of the Strength of Proximal Femur In Vitro: Relationship to Femoral Bone Mineral Density and Femoral Geometry,» *Bone,* vol. 20, n. 3, pp. 213-218, March 1997.

[60] B. Cohen and N. Rushton, «Accuracy of DEXA measurement of bone mineral density after total hip arthroplasty,» *J Bone Joint Surg Br.,* vol. 77, n. 3, pp. 479-483, 1995.

[61] E. Mirsky and T. Einhorn, «Bone densitometry in orthopaedic practice,» *J Bone Joint Surg Am,* vol. 80, n. 11, pp. 1687-1698, 1998.

[62] R. Schmidt, L. Muller, A. Kress, H. Hirschfelder, A. Aplas and R. Pitto, «A computed tomography assessment of femoral and acetabular bone changes after total hip arthroplasty.,» *Int Orthop,* vol. 26, n. 5, pp. 299-302, 2002.

[63] R. Pitto, L. Mueller, K. Reilly, R. Schmidt and J. Munro, «Quantitative computer-assisted osteodensitometry in total hip arthroplasty,» *Int Orthop,* vol. 31, n. 4, pp. 431-438, 2006.

[64] M. Viceconti, L. Cristofolini, M. Baleani and A. Toni, «Pre-clinical validation of a new partially cemented femoral prosthesis by synergetic use of numerical and experimental methods,» *J Biomech,* vol. 34, pp. 723-732, 2001.

[65] T. Szwedowski, W. Taylor, M. Heller, C. Perka, M. Muller et al., “Generic Rules of Mechano-Regulation Combined with Subject Specific Loading Conditions Can Explain Bone Adaptation after THA,” *PLoS ONE,* vol. 7, no. 5, 2012.

[66] R. Huiskes, «Stress shielding and bone resorption in THA: clinical versus computer-simulation studies,» *Acta Orthop Belg.,* vol. 59, pp. 118-129, 1993.

[67] J. Kerner, R. Huiskes, G. van Lenthe, W. H., R. Van, C. Engh and A. Amis, «Correlation between pre-operative periprosthetic bone density and post-operative bone loss in THA can be explained by strain-adaptive remodelling,» *J Biomech,* vol. 32, pp. 695-703, 1999.

[68] E. Schileo, F. Taddei, L. Cristofolini et al., «Subject-specific finite element models implementing a maximum principal strain criterion are able to estimate failure risk and fracture location on human femurs tested in vitro,» *Journal of Biomechanics,* n. 41, pp. 356-367, 2008.

[69] T. Helgason, P. Gargiulo, P. Ingvarsson and S. Yngvason, «Using Mimics to Monitor Changes in Bone Mineral Density of Femur during Electrical Stimulation Therapy of Denervated Degenerated Thigh Muscles,» *ResearchGate.*

[70] Y. Pauchard, P. Gargiulo et al., «Assessing Bone Changes after Total Hip Arthroplasty with Computed Tomography,» in *CMBBE 2015*, Montreal, 2015.

[71] R. Radiology, «Metal Deletion Technique (MDT) - ReVision Radiology».

[72] Þ. Hermannsson and P. Gargiulo, "Phantom protocol for segmentation and bone apparent density calculation," University of Reykjavik, 2016.

[73] E. Morgan, H. Bayraktar and T. Keaveny, «Trabecular bone modulus–density relationships depend on anatomic site,» *J. Biomech.,* n. 36, pp. 897-904, 2003.

[74] A. Winter, «Amos G. Winter, Assistant Professor MIT,» 2006. [Online]. Available: web.mit.edu.

[75] G. Niemann and H. Winter, Elementi di Macchine vol. I, Springer, 1983.

[76] R. Sakai, A. Takahashi et al., «Hammering force during cementless total hip arthroplasty and risk of microfracture.,» *Hip International,* vol. 21, pp. 330-335, 2011.

[77] J. Orlik, A. Zhurov et al., «On the secondary stability of coated cementless hip replacement: parameters that affected interface strength,» *Medical Engineering & Physics,* n. 25, pp. 825-831, 2003.

[78] J. Grant, N. Bishop et al., «Artificial composite bone as a model of human trabecular bone:The implant–bone interface,» *Journal of Biomechanics,* n. 40, pp. 1158-1164, 2007.

[79] R. P. Pitto et al., «Femoral bone density changes after total hip arthroplasty with uncemented taper-design stem: a five year follow-up study,» *International Orthopaedics,* n. 34, pp. 783-787, 2010.

[80] P. Gargiulo, T. Pétursson, B. Magnússon, P. Bifulco et al., «Assessment of Total Hip Arthroplasty by Means of Computed Tomography 3D Models and Fracture Risk Evaluation,» *Artificial Organs,* 2013.

[81] J. Sanchez-Sotelo, D. Lewallen, W. Harmsen and J. Harrington, «Comparison of wear and osteolysis in hip replacement using two different coatings of the femoral stem.,» *Int Orthop,* vol. 28, pp. 206-210, 2004.

[82] F. Taddei, E. Schileo, B. Helgason, L. Cristofolini and M. Viceconti, «The material mapping strategy influences the accuracy of CT-based finite element models of bones: An evaluationagainst experimental measurements,» *Medical Engineering & Physics,* vol. 23, pp. 973-979, 2007.

[83] B. Helgason, F. Taddei, H. Palsson, E. Schileo, L. Cristofolini, M. Viceconti and S. Brynjolfsson, «A modified method for assigning material properties to FE models of

bones,» *Medical Engineering & Physics,* vol. 30, pp. 444-453, 2008.

[84] S. H. Pettersen, T. S. Wik and B. Skallerud, «Subject specific finite element analysis of stress shielding around cementless femoral stem,» *Clinical Biomechanics,* vol. 24, pp. 196-202, 2009.

[85] B. van Rietbergen, R. Huiskes, H. Weinans et al., “The mechanism of bone remodeling and resorption around press-fitted THA stems,” *J Biomech,* p. 26, 1993.

[86] Zimmer, «The CLS® Spotorno® Stem,» 2008.

[87] T. A. -. T. P. a. Applications, “AZO Materials,” [Online]. Available: http://www.azom.com/properties.aspx?ArticleID=2064.

[88] G. M. Izzo, Support for total hip replacement surgery: structures modeling, gait data analysis and reporting systems, Reykjavik, Napoli: Reykjavik University; Scuola di Ingegneria Federico II Napoli, 2012.

[89] K. T. Mäkelä, A. Eskelinen, P. Paavolainen, P. Pulkkinen and V. Remes, «Cementless total hip arthroplasty for primary osteoarthritis in patients aged 55 years and older: Results of the 8 most common cementless designs compared to cemented reference implants in the Finnish Arthroplasty Register,» *Acta Orthopaedica,* vol. 81, n. 1, pp. 42-52, 2010.

Appendix A-1

The CLS® Spotorno® Stem

This cementless stem, with its characteristic three-dimensional wedge shape and sharpened ribs in the proximal region, was launched in its first version in1984. Over 20 years of extensively documented clinical results and over 500 000 implants (as of 2007) demonstrate the success and confirm the exceptional properties and safety of this system. [86]

Main characteristics are:

- Three-dimensional taper and trapezoid cross-section to provide proximal transmission of the loads and to guarantee excellent primary and rotational stability;
- Ribs in the proximal region designed with sharp edges to facilitate the introduction of the stem in the bone. The sharp edges also promote cancellous bone growth between the ribs and a greater bone compression, which leads to an increased stimulus for bone formation;
- Titanium alloy (Protasul-100, Ti-6Al-7Nb) material, which is largely osteophilic. The surface is rough (grit-blasted) for a better osseointegration and to promote formation of new trabecular bone.

Figure A-1 : The Zimmer's CLS® Spotorno® Stem [86]

Material properties of Ti-6Al-7Nb are resumed in Table A-1:

Property	Value
Density	4.52 g/cm^3
Ultimate Tensile Strength	1000 MPa
Tensile Yield Strength	900 MPa
Young's Modulus	105 000 MPa
Poisson's Ratio	0.35
Surface Roughness (grit-blasted)	4-6 µm

Table A-1 : Properties of Protasul-100 (Ti-6Al-7Nb) [87]

Acknowledgments

I would like to thank Prof. Luca Cristofolini for presenting me the possibility to take part in a study experience abroad and for his valuable suggestions during the writing of the thesis.
I would like to express my gratitude to Prof. Paolo Gargiulo for hosting me at the Reykjavik University, and for the opportunity he gave me to work on such an interesting project.
Thanks to Prof. Magnús Kjartan Gíslason for his courtesy and willingness to guide me in developing the thesis through his advices.
I would also like to thank all the people I collaborated with during the stay at the Reykjavik University, in particular Þröstur Hermannsson, Joseph Lovecchio, Margherita Maddalena and Valentina Paladino.
Last but not least, I would like to thank my family for their fundamental support with words and deeds during all these University years.